An intercomparison of HO₂ measurements by Fluorescence Assay by Gas Expansion and Cavity Ring–Down Spectroscopy within HIRAC (Highly Instrumented Reactor for Atmospheric Chemistry)

Lavinia Onel[1], Alexander Brennan[1], Michele Gianella[2], Grace Ronnie[1], Ana Lawry Aguila[2], Gus Hancock[2], Lisa Whalley[1,3], Paul W. Seakins[1,3], Grant A. D. Ritchie[2], Dwayne E. Heard[1,3]

[1] School of Chemistry, University of Leeds, Leeds, LS2 9JT, UK
[2] Department of Chemistry, Physical and Theoretical Chemistry Laboratory, University of Oxford, Oxford, OX1 3QZ, UK
[3] National Centre for Atmospheric Science, University of Leeds, Leeds, LS2 9JT, UK

Correspondence to: Lavinia Onel (chmlo@leeds.ac.uk); Paul Seakins (p.w.seakins@leeds.ac.uk); Grant Ritchie (grant.ritchie@chem.ox.ac.uk); Dwayne Heard (d.e.heard@leeds.ac.uk)

Abstract.

The HO₂ radical was monitored simultaneously using two independent techniques in the Leeds HIRAC atmospheric simulation chamber at room temperature and total pressures of 150 mbar and 1000 mbar of synthetic air. In the first method, HO₂ was measured indirectly following sampling through a pinhole expansion to 3 mbar when sampling from 1000 mbar and 1 mbar when sampling from 150 mbar, with subsequent addition of NO to convert it to OH which was detected via laser-induced fluorescence spectroscopy using the FAGE (fluorescence assay by gas expansion) technique. The FAGE method is used widely to measure HO₂ concentrations in the field, and was calibrated using the 185 nm photolysis of water vapour in synthetic air with a limit of detection at 1000 mbar of 1.6×10^6 molecule cm⁻³ for an averaging time of 30 s. In the second method, HO₂ was measured directly and absolutely without the need for a calibration using Cavity Ring Down Spectroscopy (CRDS) with the optical path across the entire ~ 1.4 m width of the chamber, with excitation of the first O-H overtone at 1506.43 nm using a diode laser, and with a sensitivity determined from an Allan deviation plot of 3.0×10^8 and 1.5×10^9 molecule cm⁻³ at 150 mbar and 1000 mbar, respectively, for an averaging period of 30 s. HO₂ was generated in HIRAC by the photolysis of Cl₂ using black lamps in the presence of methanol in synthetic air and was monitored by FAGE and CRDS for ~ 5–10 minute periods with the lamps on and also during the HO₂ decay after the lamps were switched off. At 1000 mbar total pressure the correlation plot of [HO₂]_FAGE versus [HO₂]_CRDS gave a gradient of 0.836 ± 0.004 for HO₂ concentrations in the range ~ 4–100 $\times 10^9$ molecule cm⁻³ while at 150 mbar total pressure the corresponding gradient was 0.903 ± 0.002 for HO₂ concentrations in the range ~ 6–750 $\times 10^8$ molecule cm⁻³. For the period after the lamps were switched off, the second-order decay of the HO₂ FAGE signal via its self-reaction was used to calculate the FAGE calibration constant for both 150 and 1000 mbar total pressure. This enabled a calibration of the FAGE method at 150 mbar, an independent measurement of the FAGE calibration at 1000 mbar, and an independent determination of the HO₂ cross section at 1506.43 nm, σ_{HO2}, at both pressures. For CRDS, the HO₂ concentration obtained using σ_{HO2} determined using previous reported spectral data for HO₂ and the kinetic decay of HO₂ method agreed to within 20 and 12 % at 150 and 1000 mbar, respectively. For the FAGE method a very good agreement (difference within 8 %) has been obtained at 1000 mbar between the water vapour calibration method and the kinetic decay of the HO₂ fluorescence signal method. This is the first intercomparison for HO₂ between FAGE and CRDS methods, and the good agreement between HO₂ concentrations measured using the indirect FAGE method and the direct CRDS method provides a validation for the FAGE method, which is used widely for field measurements of HO₂ in the atmosphere.

1 Introduction

The hydroperoxy radical, HO_2, plays a central role in the chemistry of the atmosphere (Levy, 1971) and is a significant reactive species in several media such as hydrocarbon combustion (Zador et al., 2011;Blocquet et al., 2013;Djehiche et al., 2014), atmospheric pressure plasmas (Gianella et al., 2016) and dielectric barrier discharges used to remove volatile organic compounds (VOCs) in air (Blin-Simiand et al., 2016). In the troposphere, HO_2 is generated directly by the reaction of OH radical with CO in the presence of O_2 (R1) and indirectly by the oxidation of larger VOCs (Reactions R2–R4) (Lu et al., 2012).

$$OH + CO\ (+ O_2) \rightarrow HO_2 + CO_2 \tag{R1}$$
$$RH + OH\ (+ O_2) \rightarrow RO_2 + H_2O \qquad (R = \text{organic group}) \tag{R2}$$
$$RO_2 + NO \rightarrow RO + NO_2 \tag{R3}$$
$$RO + O_2 \rightarrow R'O + HO_2 \tag{R4}$$
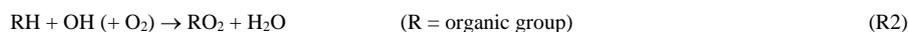
Ambient concentrations of HO_2 have been measured in a number of field campaigns and it has been found that maximum daytime concentrations are typically a few 10^8 molecule cm^{-3} (Stone et al., 2012;Heard and Pilling, 2003). With a typical lifetime in clean air of ~ 1–2 min, HO_2 radicals participate in rapid chemical cycling at the heart of tropospheric oxidation, hence HO_2 is one of the best targets for chemical models to compare with field data. HO_2 is converted back to OH through several different pathways. In unpolluted environments, its self-reaction and reaction with RO_2 are the major loss pathways for HO_2 via Reactions (R5) + (R6) and (R7):

$$HO_2 + HO_2 \rightarrow H_2O_2 + O_2 \tag{R5}$$
$$HO_2 + HO_2 + M \rightarrow H_2O_2 + O_2 + M \qquad (M = N_2 \text{ or } O_2) \tag{R6}$$
$$HO_2 + RO_2 \rightarrow ROOH + O_2 \tag{R7}$$
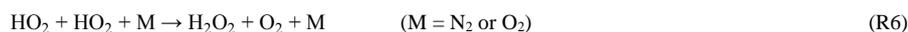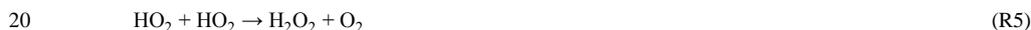
The reaction of HO_2 with NO dominates HO_2 loss in anthropogenically influenced environments and constitutes the main tropospheric *in situ* source of O_3 by Reactions (R8)–(R10).

$$HO_2 + NO \rightarrow OH + NO_2 \tag{R8}$$
$$NO_2 + h\nu\ (\lambda < 420\ nm) \rightarrow NO + O(^3P) \tag{R9}$$
$$O(^3P) + O_2 + M \rightarrow O_3 + M \tag{R10}$$

In the marine boundary layer the reaction of HO_2 with halogen oxides, XO (X = Br, I), is also an important OH regeneration reaction (Bloss et al., 2005) :

$$HO_2 + XO \rightarrow HOX + O_2 \tag{R11}$$
$$HOX + h\nu \rightarrow OH + X \tag{R12}$$

In addition, OH can be reformed from HO_2 via the relatively slow reaction with ozone:

$$HO_2 + O_3 \rightarrow OH + 2O_2 \tag{R13}$$

Because of its importance in various environments, HO_2 has been measured in laboratory experiments by a variety of spectroscopic methods. Early laboratory work studying the kinetics of HO_2 reactions used UV absorption near 220 nm to

monitor HO$_2$ with detection limits of ~ 6×10^{11} molecule cm^{-3} (Kircher and Sander, 1984). The absorption spectrum of HO$_2$ in this region is broad, structureless and often overlapped by other species present in the system, such as RO$_2$ radicals and H$_2$O$_2$ (produced by the HO$_2$ self-reaction (Reactions (R5) + (R6)), hence UV absorption spectroscopy is a relatively unselective technique. As the HO$_2$ absorption spectrum in the infrared (IR) is more structured than in the UV region, the selectivity of the

5 IR absorption methods is higher. Although the near IR range offers weaker absorption bands than the fundamental vibrational bands in the mid IR region (Yamada et al., 1983;Zahniser and Stanton, 1984) near IR lasers, detectors and optical components offer an improved performance over those in the mid IR. Therefore, more recent advances in the direct detection of HO$_2$ have been made by the development of absorption techniques in the near IR, typically using diode laser absorption via the first vibrational overtone of the O-H stretch, to monitor HO$_2$ by cavity absorption methods (Djehiche et al., 2011;Djehiche et al.,

10 2014;Gianella et al., 2016;Bell et al., 2012) or conventional multi-pass/long-pass absorption spectroscopy (Tang et al., 2010) sometimes in combination with wavelength modulation spectroscopy (Taatjes and Oh, 1997;Christensen et al., 2004) or two-tone frequency modulation spectroscopy (Schocker et al., 2007;DeSain et al., 2003). The use of methods such as frequency modulation and intracavity absorption improves sensitivity, with typical detection limits in the range ~10^9–10^{11} molecule cm^{-3}. A recent addition to the spectroscopic techniques used for HO$_2$ detection in laboratory is mid IR Faraday rotation spectroscopy,

15 which has been employed for *in situ* measurements of HO$_2$ at atmospheric pressure in combustion studies using dimethyl ether to obtain a 1σ concentration detection limit of 0.1 ppmv (1.15×10^{12} molecule cm^{-3} at 623 K) (Brumfield et al., 2013;Kurimoto et al., 2015). Whilst allowing wide applications for spectroscopic and kinetic applications these detection limits do not allow for the detection of HO$_2$ under atmospheric conditions where concentrations are typically around 10^8 molecule cm^{-3} (Heard and Pilling, 2003).

20 Cavity ring-down spectroscopy (CRDS) using the OH overtone vibrational band (2,0,0)–(0,0,0) of the ground electronic state $\tilde{X}^2A$" (the $2\nu_1$ band is centred at 6648.9 cm^{-1} *i.e.* ~ 1504 nm (Thiebaud et al., 2007)) of HO$_2$ has been applied in a number of studies to detect HO$_2$ at reduced pressure (Djehiche et al., 2014;Liu et al., 2008). The CRDS technique (Brown, 2003;O'Keefe and Deacon, 1988;Wheeler et al., 1998) is well established and consists in trapping a laser beam within a high finesse optical resonator formed by two highly reflective dielectric mirrors. If the laser frequency matches one of the cavity

25 resonance frequencies, optical power within the resonator quickly builds up, and a fraction of the circulating power leaks out through one mirror. When the light intensity exiting the cavity exceeds a certain threshold, the laser beam is switched off abruptly and the intensity decays exponentially ('ring-down') with a time constant that is a measure of the cavity losses. If an absorbing gas is introduced into the cavity, the ring-down time will decrease due to the additional absorption loss. The concentration of the absorbing species, [A], is related to the difference in ring-down times via (O'Keefe and Deacon, 1988):

30 $$[A] = \frac{1}{\sigma c}\left(\frac{1}{\tau} - \frac{1}{\tau_0}\right), \tag{1}$$

where σ is the absorption cross section of the species A, c is the velocity of light, τ and τ_0 are the ring-down times in the presence and absence of the absorber.

Fittschen and co-workers have used the CRDS technique to perform time-resolved measurements of the HO$_2$ radicals, generated by pulsed laser photolysis in a flow cell, to extract spectroscopic (Thiebaud et al., 2007;Thiebaud and Fittschen,

35 2006;Ibrahim et al., 2007;Parker et al., 2011) and kinetic (Thiebaud and Fittschen, 2006;Morajkar et al., 2014) information. The experiments have been conducted at room temperature to provide absorption cross sections and spectral line strengths at 50 Torr of He (Thiebaud et al., 2007;Parker et al., 2011) and air-broadening coefficients of the spectral lines (Ibrahim et al., 2007) (by using pressures between 7 and 160 Torr) for HO$_2$ in the $2\nu_1$ band. The most significant absorption feature in the wavelength range 6604 – 6696 cm^{-1} has been found at 6638.20 cm^{-1} (*i.e.* 1506.43 nm), with a Doppler limited peak cross

40 section of $\sigma_D = 4.2 \times 10^{-19}$ cm^2 molecule^{-1} (no errors quoted), in very good agreement with the conventional multi-pass study performed by Tang et al. (2010)., which reports $\sigma_D = (4.3 \pm 1.1) \times 10^{-19}$ cm^2 molecule^{-1} at the same wavenumber. Fittschen

and co-workers calculated a minimum detectable concentration of HO_2 of 3.2×10^9 molecule cm^{-3} for detection at 6638.20 cm^{-1} with a 1 Hz detection bandwidth (1 s integration time) (Thiebaud et al., 2008).

Despite its significance, at present HO_2 is not typically measured directly in the atmosphere. Previous direct measurements of HO_2 were performed by the Matrix Isolation Electron Spin Resonance (MIESR) technique (Mihelcic et al., 1978), but this

5   method has been retired and was characterised by long time averaging times (30 min (Fuchs et al., 2009)). However, recently Chemical Ionisation Mass Spectrometry (CIMS) employing Br^- as a reagent ion has been used for direct HO_2 measurements with a limit of detection of $\sim 1.7 \times 10^7$ molecule cm^{-3} for a 1 min integration time (Sanchez et al., 2016). Laser-induced fluorescence (LIF) at low pressure, known as Fluorescence Assay by Gas Expansion (FAGE) (Stone et al., 2012;Heard and Pilling, 2003), is most commonly used for the measurements of OH and HO_2. However, HO_2 is not detected directly, rather it

10 is converted to OH by reaction with added NO (R8) followed by OH on-resonance LIF at 308 nm (Hard et al., 1992). FAGE is a sensitive technique, with a typical detection limit for HO_2 of $(5–10) \times 10^5$ molecule cm^{-3}, depending on the individual instrument, averaging time and the desired signal-to-noise ratio (Stone et al., 2012). Another indirect method uses CIMS to determine the sum of HO_2 and the organic peroxy radicals (RO_2), $[HO_2] + \sum_i[RO_{2,i}]$, or separately $[HO_2]$ depending on the flows of the NO and SO_2 reagents (Hanke et al., 2002;Edwards et al., 2003). A typical detection limit for the indirect CIMS

15 (sometimes referred to as per-CIMS or ROXMAS) method is 1×10^7 molecule cm^{-3} for 15 s averaging time (Hanke et al., 2002;Edwards et al., 2003). The HO_2 concentrations at an urban site have also been recently derived from observations of HO_2NO_2 by using CIMS with $I^- \cdot (H_2O)_n$ as a reagent ion combined with measurements of NO_2 by cavity attenuated phase shift spectroscopy (Chen et al., 2017). The Peroxy Radical Chemical Amplifier (PERCA) method has been used for many years to determine the sum $[HO_2] + \sum_i[RO_{2,i}]$ by using NO and CO to generate NO_2, which is amplified by a chain reaction and

20 subsequently measured through a range of methods, such as luminol fluorescence, LIF or cavity absorption methods, with typical detection limits in the range of $1–2.5 \times 10^7$ molecule cm^{-3} in a 1 min time-period (Cantrell and Stedman, 1982;Cantrell et al., 1984;Miyazaki et al., 2010;Green et al., 2006;Chen et al., 2016). A recently developed method is RO_xLIF, which is an extension of FAGE, enabling HO_2 and $\sum_i[RO_{2,i}]$ to be measured separately (Fuchs et al., 2008), and with good sensitivity ($\sim 2.5 \times 10^6$ molecule cm^{-3} detection limit in 1 min). The concentration of the initial HO_2 is determined by subtracting the separate

25 direct measurement of [OH] from the indirect measurement of $[HO_x] = [OH] + [HO_2]$ by converting HO_x to HO_2 through addition of CO followed by the HO_2 conversion into OH in the FAGE detection chamber.

Whilst FAGE has the appropriate sensitivity and time resolution for atmospheric monitoring, there are two issues that could potentially cause systematic errors with this technique. First, FAGE is not an absolute method and hence requires a calibration which may lead to a source of error. Secondly, it is not a direct technique, but requires chemical conversion to another species,

30 OH, which is subsequently detected by LIF spectroscopy, and hence may be subject to additional uncertainties associated with the conversion, i.e. could be prone to interferences arrising from the conversion of species other than HO2 to OH. One known interference of this type is the conversion of beta-hydroxyalkylperoxy radicals (Fuchs et al., 2011;Whalley et al., 2013). For calibration, the most common method to generate accurate known concentrations of OH and HO_2 uses the photolysis of water vapour at 184.9 nm in zero air employing a mercury pen-ray lamp:

35

$$H_2O \xrightarrow{184.9\ nm} OH + H \qquad\qquad\qquad\qquad\qquad\qquad\qquad (R14)$$

$$H + O_2 + M \rightarrow HO_2 + M, \qquad\qquad\qquad\qquad\qquad\qquad\qquad (R15)$$

The water photolysis method has been used for many years for the calibration of FAGE instruments (Stone et al., 2012;Heard

40 and Pilling, 2003). The reliability of the method has been confirmed by intercomparisons with alternative methods of calibration for OH and HO_2. For HO_2, the kinetics of the second-order decay of HO_2 via its self-reaction has been observed in HIRAC (Highly Instrumented Reactor for Atmospheric Chemistry) to obtain a FAGE calibration factor in good agreement

with the one determined by using the water photolysis method for a pressure in the fluorescence detection cell between 1.4–3.8 mbar (Winiberg et al., 2015).

Intercomparisons between different HO_2 instruments have been used to probe the susceptibility of instruments towards any bias, for example via the calibration methodology used and potential interferences. In 2005, three FAGE instruments measured

5   HO_2 during the HO$_x$Comp campaign, showing variable agreement with correlation slopes between 0.69 to 1.26 in the SAPHIR (Simulation of Atmospheric Photochemistry in a large Reaction Chamber) chamber and sometimes worse correlations in ambient air (Fuchs et al., 2010). Agreement whilst detecting HO_2 in the same location for various designs of the FAGE technique increases the confidence in the use of the FAGE method, but such intercomparisons are rare. A field intercomparison between FAGE and CIMS measurements of HO_2 gave agreement within 40% (Ren et al., 2003) while a subsequent

10   intercomparison between RO$_x$LIF and MIESR techniques for HO_2 in the SAPHIR chamber resulted in a very good agreement, with correlation slopes of 0.98 ± 0.08 (1σ) (Fuchs et al., 2009).

This paper reports the first intercomparison between FAGE and CRDS measurements of HO_2. The experiments have been performed at room temperature and two different pressures: 150 mbar and 1000 mbar within the HIRAC atmospheric simulation chamber (Glowacki et al., 2007). For measurements at 1000 mbar, FAGE was calibrated using the conventional

15   water vapour photolysis method, whilst at 150 mbar the FAGE calibration constant was determined by studying the kinetics of HO_2 via its self-reaction, where the time constant of the second-order decay depends on the absolute, initial concentration of HO_2, $[HO_2]_0$. The CRDS technique was chosen as a reference for the validation of the HO_2 FAGE method as CRDS is an absolute absorption method and hence requires no calibration. Reported here are the first CRDS measurements of HO_2 carried out in an atmospheric simulation chamber. The newly constructed CRDS spectrometer consists of a high finesse linear optical

20   cavity set up across the chamber for the *in situ* direct HO_2 detection over a distance of ~ 1.4 m between two highly reflective dielectric mirrors (R > 0.9999; typical ring-down time $\tau = 230$ μs), which results in ~ 70 km effective absorption path length. The use of a homogeneously mixed chamber allowed the same $[HO_2]$ to be sampled by the two techniques. A further advantage of the use of HIRAC is that the experiments can be performed under controlled conditions which produce approximately constant $[HO_2]$ at different levels and, in addition, can generate HO_2 temporal decays by turning off the UV lamps employed

25   for the generation of the radicals in the chamber. The CRDS spectrometer used diode laser light at 1506.43 nm (vacuum wavelength, corresponding to 6638.2 cm^{-1}) to probe HO_2 at its peak absorption in the $2\nu_1$ band. The HO_2 cross sections at 1506.43 nm, σ_{HO2}, at 150 mbar and 1000 mbar, respectively are estimated using the reported HO_2 spectra and pressure-broadening coefficients for the transitions contributing to σ_{HO2} (Thiebaud et al., 2007) and are compared with values obtained by analysing the second-order temporal decays of HO_2 monitored by CRDS and FAGE.

30

2 Experimental

2.1 HO_2 generation in HIRAC

Experiments were conducted in HIRAC, at 295 K and in 150 mbar and 1000 mbar of synthetic air obtained by mixing high purity oxygen (BOC, > 99.999 %) and nitrogen (BOC, > 99.998 %) in the ratio of $O_2:N_2 = 1:4$. HIRAC is a stainless steel

35   cylinder with internal dimensions of 2.0 m length and 1.2 m diameter (Fig. 2a below), which was built with a number of flanges to allow for easy coupling of equipment and has been described in detail previously (Glowacki et al., 2007). Thorough mixing of the gas mixtures was achieved by four low-vibration circulation fans mounted in pairs at each end of the chamber. Methanol (Sigma Aldrich, HPLC grade, ≥ 99.9 %, $(0.7 - 1.4) \times 10^{14}$ molecule cm^{-3} in the experiments at 150 mbar and $(0.8 - 2.0) \times 10^{14}$ molecule cm^{-3} in the experiments at 1000 mbar) and molecular chlorine (Sigma Aldrich, ≥ 99.5 %, $7 \times 10^{12} - 2.1 \times 10^{14}$

40   molecule cm^{-3} in the experiments at 150 mbar and $(0.4 - 1.6) \times 10^{14}$ molecule cm^{-3} in the experiments at 1000 mbar) were delivered to the chamber. The chemistry generating HO_2 was initiated by the photolysis of Cl_2 using eight UV black lamps

(Phillips, TL-D36W/BLB, λ = 350–400 nm) housed in quartz tubes mounted radially inside the reactive volume (aligned parallel to the chamber longitudinal axis):

$$Cl_2 \xrightarrow{h\nu} Cl + Cl \qquad\qquad\qquad (R16)$$

5 $$CH_3OH + Cl \rightarrow CH_2OH + HCl \qquad\qquad\qquad (R17)$$

$$CH_2OH + O_2 \rightarrow HO_2 + CH_2O \qquad\qquad\qquad (R18)$$

Two kinds of intercomparison studies have been performed: experiments where the UV lamps were turned on for 5 – 10 min to generate a slowly changing [HO_2] and then off to follow the HO_2 decay (Sect. 3.5) and experiments where the lamps were

10 alternately turned on for 2 – 3 min and then off for ~ 3 min to generate a series of three HO_2 temporal decays followed by regeneration of the HO_2. Figures S7 and S8 in the supplementary information are examples of the series of HO_2 decays measured at the two pressures.

2.2 FAGE instrument

15 Full details on the HIRAC FAGE instrument can be found in previous publications (Winiberg et al., 2016;Onel et al., 2017;Winiberg et al., 2015). In the FAGE method, gas was sampled from the HIRAC chamber via 50 mm diameter sampling inlet into a reduced pressure fluorescence cell where OH (either present in the HIRAC chamber or converted from HO_2) was detected by LIF. Although capable of simultaneously determining OH and HO_2, only data from the HO_2 measurements are described here.

20 In order to detect the HO_2 radicals generated within HIRAC the FAGE instrument was coupled to the chamber through a custom-made ISO-K160 flange to sample the gas at ~ 230 mm from the chamber wall (Fig. 2a in Sect. 2.4). Under typical operating conditions, air was sampled at ~ 3 slm through a 1.0 mm diameter pinhole nozzle and passed down the inlet (length 280 mm, 50 mm diameter, although the length was varied in some experiments, see below) into the OH detection axis maintained at low pressure using a high capacity rotary pump-backed roots blower pumping system (Leybold, trivac D40B

25 and ruvac WAU251). Concentrations of HO_2 were measured simultaneously in a second detection axis ~300 mm downstream of the OH detection axis (internal pressure = (3.24 ± 0.20) mbar when sampling from 1000 mbar). High purity NO (BOC, N2.5 nitric oxide) was added ~25 mm before the HO_2 detection axis into the centre of the FAGE cell in the direction of gas flow through 1/8"diameter stainless steel tubing at a rate of 2.5 sccm (Brooks 5850S) converting a fraction of HO_2 to OH. LIF with excitation at 308 nm ($A^2\Sigma^+$ (v'=0) ← $X^2\Pi_i$ (v"=0) transition) was used to probe the OH radicals directly, and the resulting

30 fluorescence was collected after passing through an interference filter (308.8 ± 5.0 nm). Laser light was generated using a pulsed Nd:YAG (JDSU Q201-HD) pumped dye laser (SIRAH Credo-Dye-N) operating at 5 kHz pulse repetition frequency and delivered via fibre optics to the fluorescence and reference cells. The laser power entering the HO_2 fluorescence cell was typically 3 – 5 mW. A small portion of the laser light was directed into a reference cell where high concentrations of OH were generated from the thermal dissociation of water. The use of a reference cell maintained the laser at the optimum wavelength

35 and the laser power reaching the reference cell was monitored to allow normalization of the fluorescence signal to fluctuations in laser power.

2.3 FAGE calibration for HO₂

2.3.1 Calibration at atmospheric pressure - H₂O vapour photolysis

As described above and detailed in Winiberg et al. (2015), the photolysis of water at 184.9 nm is used to generate known concentrations of OH and HO_2. A humidified flow of zero air (40 SLM, BOC, BTCA 178) was flowed into a square cross-

5   section flow tube with [H₂O] measured using a dew-point hygrometer (CR4, Buck Research Instruments). The collimated 184.9 nm output of a mercury lamp (LOT-Oriel, Pen-Ray) was introduced to the end of the flow tube to photolyse the water. The gas output from the flow tube was directed towards the FAGE sampling inlet, where overfilling of the FAGE sampling inlet ensured no ingress of ambient air. A range of HO_x concentrations were produced by changing the lamp current. The HO_x concentrations are given by:

10         $[OH] = [HO_2] = [H_2O] \; \sigma_{H2O, \, 184.9 \, nm} \; \Phi_{H2O} \; F_{184.9 \, nm} \; \Delta t.$ (2)

where $\sigma_{H2O, \, 184.9 \, nm}$ is the photolysis cross-section of water at 184.9 nm, Φ_{OH} is the quantum yield for OH formation (unity), $F_{184.9 \, nm}$ is the photon flux and Δt is the photolysis time. The photolysis cross-section and quantum yield are well known and the product $F_{184.9 \, nm} \Delta t$ is determined by N₂O actinometry (Edwards et al., 2003). An example of a calibration plot is shown in the supplementary information (Fig. S1). The resultant average calibration constant was:

15   $C_{HO2} = (2.6 \pm 0.4) \times 10^{-7}$ counts cm³ molecule⁻¹ s⁻¹ mW⁻¹

where C_{HO2} is defined by $S_{HO_2} = C_{HO_2} [HO_2]$ and the error is a combination of systematic and statistical uncertainties at the 1σ level. The resulting limit of detection (LOD) for a signal-to-noise ratio (S/N) of 2 and 2 minute averaging, was $LOD = 7.8 \times 10^5$ molecule cm⁻³. The value of the calibration constant is in very good agreement with the value obtained by using the kinetic decay method based on determination of HO₂ second-order recombination (Sect. S2 in the supplementary information and

20   (Winiberg et al., 2015)) at 1000 mbar, which gives: $C_{HO2} = (2.4 \pm 0.5) \times 10^{-7}$ counts cm³ molecule⁻¹ s⁻¹ mW⁻¹. The principle behind the kinetic method of calibration is that the time constant of the second-order decay of HO₂ in the self-reaction is dependent upon its initial concentration, and hence its analysis offers an alternative way to calibrate the signal. Winiberg et al. have shown that C_{HO2} is relatively invariant between the high water vapour concentrations of the flow tube calibration method ([H₂O] ~ 7 × 10¹⁶ molecule cm⁻³) and the relatively dry conditions in HIRAC ([H₂O] ~ 10¹³ – 10¹⁴ molecule cm⁻³) for the HO₂

25   recombination method. Therefore, the average value of these methods is: $\overline{C}_{HO2, \, 1000 \, mbar} = (2.5 \pm 0.5) \times 10^{-7}$ counts cm³ molecule⁻¹ s⁻¹ mW⁻¹.

2.3.2 Calibration at 150 mbar - kinetics of the HO₂ temporal decay

The kinetics of the temporal decay of HO₂ has been used as the calibration method of FAGE sampling from HIRAC at 150

30   mbar (fluorescence cell pressure = (1.0 ± 0.1) mbar). This method was previously validated for HO₂ in HIRAC, where the FAGE calibration constant, C_{HO2}, obtained from the analysis of the temporal decay of HO₂ (generated by the photolysis of HCHO, then the chamber lamps switched off) agreed with C_{HO2} from the conventional water vapour photolysis method for a range of pressures in the fluorescence detection cell, 1.3–3.9 mbar (Winiberg et al., 2015). The variation of C_{HO2} is small and linear and therefore the uncertainties associated with the short extrapolation for the internal cell pressure of 1.3 to 1.0 mbar are

35   small.

In order to generate the second-order decays the chamber photolysis lamps were turned off. The HO₂ was consumed by the bimolecular and termolecular self-reactions (Reactions (R5) + (R6)) and removed by the first-order wall-loss. In order to investigate if HO₂ removal by the wall-loss is significant, the experimental data were fitted by two different equations. Eq. (3)

assumes that the loss of HO_2 is due entirely to the overall self-reaction (Reactions (R5) + (R6)), i.e. without taking into account the wall-loss of HO_2.

$$(S_{HO_2})_t = \left(\frac{1}{(S_{HO_2})_0} + \frac{2 \cdot k_{self-r.} t}{C_{HO_2}} \right)^{-1} ,$$ (3)

where $(S_{HO2})_t$ is the fluorescence signal at reaction time t, $(S_{HO2})_0$ is the signal at time $t = 0$, when the lamps were switched off and $k_{self-r.}$ is the overall HO_2 self-reaction rate coefficient. Eq. (4) includes the HO_2 wall-loss as a first-order process:

$$(S_{HO_2})_t = \left(\left(\frac{1}{(S_{HO_2})_0} + \frac{2 \cdot k_{self-r.}}{k_{loss} \cdot C_{HO_2}} \right) \times \exp(k_{loss} t) - \left(\frac{2 \cdot k_{self-r.}}{k_{loss} \cdot C_{HO_2}} \right) \right)^{-1} ,$$ (4)

where k_{loss} is the rate coefficient describing the HO_2 wall-loss.

Figure 1 shows an example of the experimental decay of S_{HO2} with data averaged over 0.1 second (500 laser pulses) and the fits given by equations (3) and (4) above fixing $k_{self-r.}$ to 1.79×10^{-12} cm^3 molecule^{-1} s^{-1}, according to the IUPAC recommendation (Atkinson et al., 2004), and with C_{HO2} and k_{loss} floated. It is clear that wall-losses must be included in order

15 to provide a good fit to the data, especially at later times ($r^2 = 0.99$). This result is in agreement with previous HO_2 calibrations where Eq. (4) was applied to analyse the kinetics of the HO_2 decays generated in HIRAC (Winiberg et al., 2015). Therefore, Eq. (4) has been chosen to fit the experimental data. Nine HO_2 decays were analysed, which yielded an average value of C_{HO2} = $(2.6 \pm 0.5) \times 10^{-7}$ counts cm^3 molecule^{-1} s^{-1} mW^{-1}. Therefore, $C_{HO2, \, 150 \, mbar} \cong C_{HO2, \, 1000 \, mbar}$ ($\overline{C}_{HO2, \, 1000 \, mbar}$=$(2.5 \pm 0.5) \times 10^{-7}$ counts cm^3 molecule^{-1} s^{-1} mW^{-1}; Sect. 2.3.1) which agrees with the negligible change in C_{HO2}

20 with the decrease in the detection cell pressure found previously (Winiberg et al., 2015).

The wall-loss rate coefficient obtained from the fit, $k_{loss} = (0.09 \pm 0.02)$ s^{-1}, has overlapping error limits with the range of values reported previously for HO_2 in HIRAC, (0.03–0.07) s^{-1} (Winiberg et al., 2015). Note that the parameter k_{loss} is dependent on the chamber conditions during the experiment and decreases with increasing pressure as expected for diffusive loss being the rate determining step in the wall-loss process; a value of $k_{loss} = (0.04 \pm 0.01)$ s^{-1}, has been obtained by the kinetic analysis

25 of the FAGE signal decays measured at 1000 mbar in HIRAC in this work.
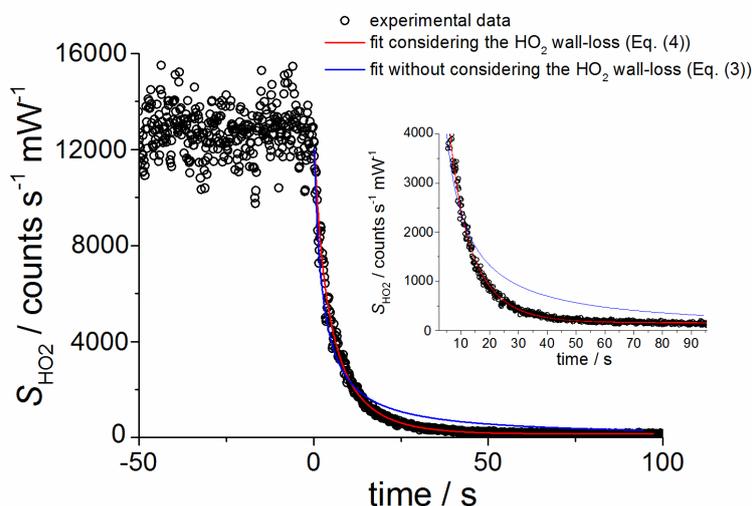
Figure 1. An example of temporal decay of the normalized FAGE HO_2 signal with 0.1 second time resolution recorded at 295 K and 150 mbar mixture of $N_2:O_2 = 4:1$ using Cl_2/CH_3OH and the black lamps (details given in the main text); $[Cl_2]_0 \sim 3 \times 10^{13}$ molecule cm^{-1} and $[CH_3OH]_0 \sim 5 \times 10^{13}$ molecule cm^{-3}. At time zero the photolysis lamps were turned off. Fitting Eq. (4) to this example trace (red line) gave $C_{HO2} = (2.45 \pm 0.06) \times 10^{-7}$ counts cm^3 molecule^{-1} s^{-1} mW^{-1} ($r^2 = 0.99$) while fitting Eq. (3) to the data (blue line) led to $C_{HO2} = (1.06 \pm 0.02) \times 10^{-7}$ counts cm^3 molecule^{-1} s^{-1} mW^{-1} ($r^2 = 0.95$) - statistical errors at 1σ level. The inset shows the fit to the data using the two equations at later times. Note that the most significant source of the signal noise is the shot noise (Poisson noise), which grows with the number of photons counted by the detector.

2.3.3 FAGE measurements of HO_2 across the HIRAC diameter

In order to ensure that the point measurements of $[HO_2]$ with FAGE and the CRDS measurements of the average $[HO_2]$ across the width of the chamber (see Section 2.4) are comparable, investigations into any $[HO_2]$ gradient across the ~ 600 mm radius of the chamber were performed. HO_2 was generated either from the photolysis of formaldehyde at 270–320 nm (lamps: Philips TL40W/12 RS) in air at 150 mbar, which produced HO_2 by the reaction of O_2 with the H atoms and the HCO radicals generated by CH_2O photolysis, or O_3 photolysis at 254 nm (lamps: GE G55T8 / OH 7G) followed by the reaction of the $O(^1D)$ generated with H_2O to produce OH and, then by the reaction of OH with O_3 at 1000 mbar of air. An extended FAGE inlet of a length of ~ 520 mm was used to sample at separate locations up to 500 mm across HIRAC. At both pressures a constant $[HO_2]$ was found (within the 10% 1σ precision uncertainty of the measurement) at locations between ~ 100 and 500 mm from the wall while $[HO_2]$ gradually decreased between ~ 100 and 0 mm from the wall; the maximum $\sim 16\%$ decrease occurred when the sampling pinhole was flush with the wall. This result is in good agreement with previous studies (Winiberg et al., 2015) and means that the point measurements of the FAGE system can readily be compared with the CRDS results. In addition, investigations into the radiation field profile within HIRAC have been performed to show that the distribution of the light intensity varies by less than 15% in $\sim 75\%$ the chamber volume (Glowacki et al., 2007).

2.4 CRDS set-up

The CRDS spectrometer was set-up across the HIRAC diameter as shown in Fig. 2. To probe HO_2, a diode laser beam at ~ 1506 nm is sent diametrically across the chamber (Fig. 2a). On either side there is a blank flange (ISO-K 500 on the injection side, ISO-K 160 on the detection side) onto which KF25 flanges have been welded so that a pair of home-made mirror mounts

can be attached. A sketch of the cavity ring-down spectrometer is given in Fig. 2b. The $\lambda \sim 1.5$ μm distributed feedback (DFB) fibre pig-tailed diode laser [A] (NTT Electronics, NLK1S5GAAA) is held in a butterfly laser diode mount (Thorlabs LM14S2). Current to the laser diode and the built-in thermoelectric element is provided by a Thorlabs ITC502 driver. The single-mode fibre is connected to an inline optical isolator [B] (Thorlabs IO-H-1505APC), an acousto-optic modulator [C] (AOM, Gooch

5 & Housego Fibre-Q T-M040-0.5C8J-3-F2S), and an adjustable fibre collimation package [D] (Thorlabs CFC-8X-C). The AOM is powered by a 0.5 W 40 MHz radio-frequency driver (Goch & Housego A35040-0.5W). The components [A], [B] and [C] lie on a small optical breadboard plate attached to HIRAC's support frame under the ISO-K 500 flange.

The free-space components [D], [E1], [E2] and [F] on the beam injection side (of the cavity) and [E3], [H], and [J] on the detection side are assembled with Thorlabs' 30-mm cage system, which in turn is supported by posts clamped onto HIRAC

10 itself. This solution mitigates misalignment of the cavity axis relative to the beam axis under the effect of the mechanical deformation (pressure difference) of HIRAC and low-vibrations caused by the chamber's circulating fans. After the fibre collimator [D], a protected silver mirror [E1] (Thorlabs PF10-03-P01) is followed by a $f = 250$ mm mode-matching lens [F] (Thorlabs LA1461-C) and a second identical mirror [E2]. The 1-inch diameter cavity mirrors [G1] and [G2] (Layertec, reflectivity: $R > 0.9999$, curvature radius: 1 m; the mode diameter varies from ~1 mm in the centre of the chamber to ~1.7 mm

15 at the cavity mirrors) are housed in a pair of home-built mounts, which allow the mirrors to tilt slightly while maintaining a gas-tight seal. The mounts are both attached to KF25 flanges welded onto the ISO-K 500 flange on the beam injection side and onto a smaller ISO-K 160 flange on the detection side. The mirror [G1] can be moved by a few microns along the beam's axis by means of a piezoelectric transducer. The distance between the two mirrors is approximately 1.4 m. On the detection side, the mirror [E3] (Thorlabs PF10-03-P01) is followed by a $f = 30$ mm focussing lens [H] (Thorlabs LA1805-C) and an

20 InGaAs photodiode [J] (Thorlabs DET10C/M).

A low-noise transimpedance amplifier [K] (FEMTO DLPCA-200) sends the photodiode signal to the data acquisition unit [L] (DAQ, National Instruments USB-6361) and to a home-made latched comparator [M] ("trigger box"). The comparator compares the photodiode signal with an adjustable threshold. When the signal crosses the threshold, the AOM is powered off (blocking the beam) and a trigger pulse is sent to the DAQ to start acquisition of the ring-down event. After a predefined

25 duration (typically 5 ms), the AOM is powered back on and the system is ready for the next ring-down event. The digitized data are processed by a custom LabVIEW program (National Instruments) running on a laptop [N]. The program fits all acquired ring-down events with an exponential function and can run in two modes: *fixed wavelength* and *scan*. In fixed wavelength mode, the program was set-up to save all ring-down events as a function of time. A number of filters can be applied to the processed events to exclude outliers (caused for example by a dust particle passing through the beam) or false positives

30 (when the acquisition is triggered by a transient noise spike), so that only legitimate ring-down events are taken into account. In scan mode, the wavelength of the laser is stepped (by changing the diode's temperature), each time a predefined number of ring-down events has been acquired and the mean ring-down time is determined as a function of wavelength. The laser emission wavelength has been calibrated using a wavemeter (Burleigh WA-1000). An example of the laser calibration plot (λ versus thermistor resistance) is shown in the supplementary information (Fig. S2). In addition, the calibration has been

35 confirmed by reproducing the well-known transmission spectrum of water vapour in the range ~1506.1–1506.9 nm (Richard et al., 2012) at both 150 mbar and 1000 mbar (Fig. S3 in the supplementary information).
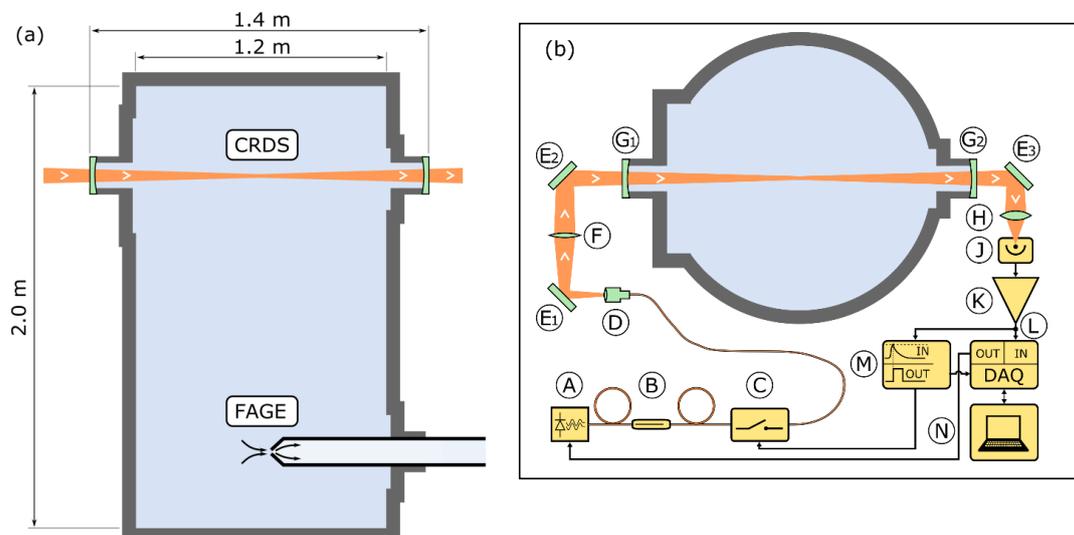
Figure 2: (a) Longitudinal (horizontal) section of HIRAC. The CRDS spectrometer probes the HO_2 concentration across the chamber's diameter, while the FAGE instrument samples the atmosphere in the chamber at one point.
(b) Cross section of HIRAC. [A] Fibre-pigtailed DFB laser diode and mount; [B] inline optical isolator; [C] acousto-optic modulator (AOM); [D] adjustable fibre collimator; [E1]-[E3] silver mirrors; [F] f = 250 mm mode-matching lens; [G1]-[G2] high reflectivity dielectric cavity mirrors; [H] f = 30 mm focusing lens; [J] InGaAs photodiode; [K] transimpedance amplifier; [L] data acquisition unit; [M] latched comparator circuitry; [N] laptop running LabVIEW for data processing and storing.

3 Results

3.1 HO_2 spectrum and comparison with literature

Figure 3 shows typical wavelength scans performed at the two HIRAC pressures. A higher spectral resolution was chosen for the measurement at 150 mbar (8×10^{-4} nm per point and averaged for 50 ring-down events per point) than for the spectral measurement at 1000 mbar (2×10^{-3} nm per point and averaged for 25 events per point) as at lower pressure the HO_2 absorption spectrum is more structured, as shown in Fig. 3, owing to reduced pressure broadening. These choices lead to a recording time of ~ 9 min at 150 mbar and 2 – 3 min at 1000 mbar. The maximum HO_2 absorption was recorded at 1506.43 nm (6638.20 cm^{-1}; Fig. 3), where the strongest HO_2 absorption line in the range ~ 1493 – 1514 nm (~ 6604 – 6696 cm^{-1}) of the first overtone of the OH stretch has been reported to lie at (Thiebaud et al., 2007). Therefore, the FAGE – CRDS intercomparison experiments were run at fixed wavelength of 1506.43 nm. The spectral feature at 1506.43 nm consists of overlapping $^qQ_3(N)$ transitions with $N = 4 – 9$, each of which is doubled by spin–rotation splitting, as originally assigned by Taatjes and co-workers (DeSain et al., 2003) who observed the absorption spectrum of the HO_2 in the $2\nu_1$ band at ~ 20 mbar of He. Next to the 1506.43 nm feature there is a weaker HO_2 absorption line at 1506.45 nm, which has been assigned to the spin-rotation split $^qP_0(6)$ transitions. As shown in Fig. 3 at 150 mbar there is little overlapping of the absorption lines, and the recorded features centred at 1506.43 nm and 1506.45 nm can be mainly attributed to the $^qQ_3(N)$ and $^qP_0(6)$ transitions, respectively. In contrast, the laser scans performed at 1000 mbar of air showed a relatively broad spectral feature centred at 1506.43 nm as the air-broadening of the HO_2 absorption lines resulted in a significant overlap of the 1506.43 nm line with the 1506.45 nm line and the other neighbouring HO_2 lines. At both pressures the minimum ring-down time, τ, occurs at 1506.43 nm. The contribution of HO_2 to the decrease in in the ring-down time at 1506.43 nm relative to τ in the absence of reagents, $\Delta\tau$ is ~ 50% at 150 mbar and ~ 20% at 1000 mbar, with the remaining contributions due to CH_3OH. During the measurements, the background absorption

decreased mainly due to the consumption of CH_3OH by the $CH_3OH + Cl$ reaction, by ~ 15% in the scan at 150 mbar and ~

10% in the scan at 1000 mbar, as determined using $[CH_3OH]$ obtained by FTIR measurements and σ_{CH3OH} determined in

separate HIRAC experiments (details in the supplementary information). The spectrum was measured from larger to smaller

wavelengths (right to left), hence the decrease in background absorption with time (decreasing λ) during a scan. The inset

5   shows an example CRDS signal at 1506.43 nm and 150 mbar and the fit to the data performed by using Eq. (5) to extract τ.

$$I_t = I_0 \exp(-\frac{t}{\tau}),\tag{5}$$

where I_t is the signal detected at time t and I_0 is the signal at $t = 0$.
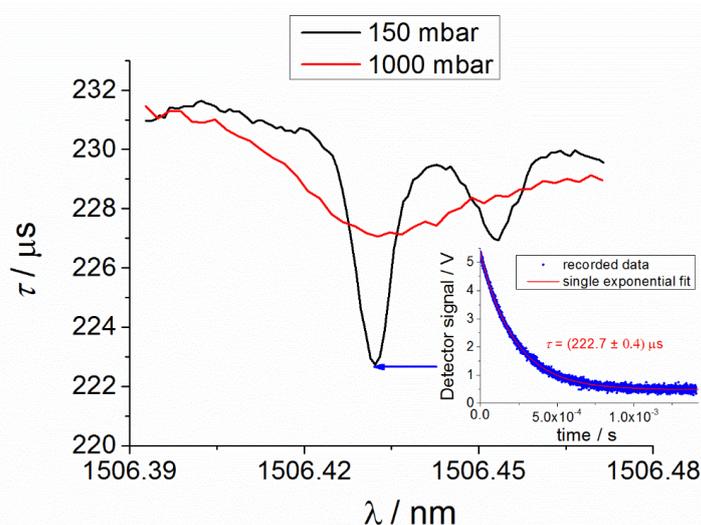
Figure 3: Typical laser scans of the ring-down time, τ, as a function of wavelength, recorded for a HIRAC pressure of 150
mbar (black line) and 1000 mbar (red line) mixture of $N_2:O_2 = 4:1$ and 295 K. For the sake of clarity the measurement at
1000 mbar was rescaled by adding 18 µs to τ. HO_2 radicals were generated in the chamber using $CH_3OH/Cl_2/O_2$ and black
15   lamps; $[CH_3OH]_0 = 7 \times 10^{13}$ molecule cm^{-3} and $[Cl_2]_0 = 4 \times 10^{13}$ molecule cm^{-3} in the experiment at 150 mbar and $[CH_3OH]_0$
$= 2 \times 10^{14}$ molecule cm^{-3} and $[Cl_2]_0 = 2 \times 10^{14}$ molecule cm^{-3} in the experiment at 1000 mbar. The number of ring-down events
averaged at each wavelength and the laser wavelength step were: 50 events and 8×10^{-4} nm (150 mbar) and 25 events and $2 \times$
10^{-3} nm (1000 mbar). The inset shows the ring-down trace acquired at 1506.43 nm and 150 mbar and the fit by Eq. (5) to
extract $\tau = (222.7 \pm 0.4)$ µs.

3.2 Determination of the absorption cross section of HO_2 at 1506.43 nm as a function of pressure

The absorption cross section of HO_2 at 1506.43 nm in the range 0–1100 mbar of air was computed by using a model which

takes into account not only the feature centred at 1506.43 nm but also the contribution of the neighbouring transitions, due to

the air-broadening of the absorption lines. The line centres v^* and strengths S (including the uncertainties δS) of the HO_2

25   transitions at 1506.43 nm and all the nearby transitions have been extracted from the spectra reported by Fittschen and co-

workers at 50 Torr of He (Thiebaud et al., 2007). The reported absorption data was scaled so that the line strength of the main

transition at 1506.43 nm becomes $S = 7.09 \times 10^{-21}$ cm^2 cm^{-1}, which we assume to be the correct value for that transition

(Fittschen, 2017). The air-broadening coefficient, γ_{air}, was assumed to be the same for all transitions,

0.115 $cm^{-1}atm^{-1} = 1.14 \times 10^{-4}$ $cm^{-1}mbar^{-1}$ (average value of 34 HO_2 transitions between 6631 and 6671 cm^{-1} (Ibrahim et

30   al., 2007)). For each transition (indexed by l), an area-normalized Voigt profile $\mathcal{V}(v;v_l^*, \Gamma_G, \Gamma_L(p))$, centred at v_l^* (here v and

v_l^* are wavenumbers) with Gaussian width Γ_G and Lorentzian width $\Gamma_L(p)$, was computed. The absorption cross section for HO$_2$ at v is then given by Eq. (6).

$$\sigma_{HO2}(v, p) = \sum_l S_l \, \mathcal{U}(v; v_l^*, \Gamma_G, \Gamma_L(p)) \qquad (6)$$

In particular, the cross section for HO$_2$ at the peak location $v_{pk} = 6638.2$ cm^{-1} (1506.43 nm) is:

$$\sigma_{HO2} = \sigma_{HO2}(v_{pk}, p) = \sum_l S_l \, \mathcal{U}(v_{pk}; v_l^*, \Gamma_G, \Gamma_L(p)). \qquad (7)$$

A plot of the calculated σ_{HO2} as a function of pressure p and at 298 K is shown in Fig. 4 for pressures ranging from 0 to 1100 mbar in steps of 50 mbar. The error bars represent the uncertainties ($\pm 1\sigma$) in σ_{HO2} arising from the uncertainties in the pressure broadening parameter, γ_{air}, and in the line strengths, S. The error caused by γ_{air} was determined by computing σ_{HO2} while linearly varying γ_{air} between the minimum and maximum value reported by Fittschen and co-workers (Ibrahim et al., 2007), i.e. between 0.078 cm^{-1}atm^{-1} and 0.155 cm^{-1}atm^{-1}. The uncertainty caused by the error in S was determined in a similar fashion, namely by computing σ_{HO2} while linearly varying the line strengths between $S_l - \delta S_l$ and $S_l + \delta S_l$. The simplest model that fits the simulated data is:

$$\sigma_{HO2}(v_{pk}, p) = A_0 + A_1 \exp(-\lambda_1 p) + A_2 \exp(-\lambda_2 p). \qquad (8)$$

The values of the fit parameters, A_0, A_1, A_2, λ_1 and λ_2, are given in Table S3 in the supplementary information.

The result of this work, $\sigma_{HO2, \, 150 \, mbar} = (1.25 \pm 0.19) \times 10^{-19}$ cm^2 molecule^{-1}, agrees very well with the value $\sigma_{HO2, \, 150 \, mbar} = (1.29 \pm 0.23) \times 10^{-19}$ cm^2 molecule^{-1} calculated by using the equation computed by Tang et al. (2010) to describe the change in σ_{HO2} at 1506.43 nm and 296 K with the increase in the pressure of air observed experimentally between 27 – 133 mbar using conventional multi-pass absorption spectroscopy. σ_{HO2} has been determined previously only at low pressures, so there is no literature value to compare with our calculated value of $\sigma_{HO2, \, 1000 \, mbar} = (3.44 \pm 0.37) \times 10^{-20}$ cm^2 molecule^{-1}. Both $\sigma_{HO2, \, 150 \, mbar}$ and $\sigma_{HO2, \, 1000 \, mbar}$ were also determined by using the kinetic method to obtain [HO$_2$] presented in Sect. 3.3.
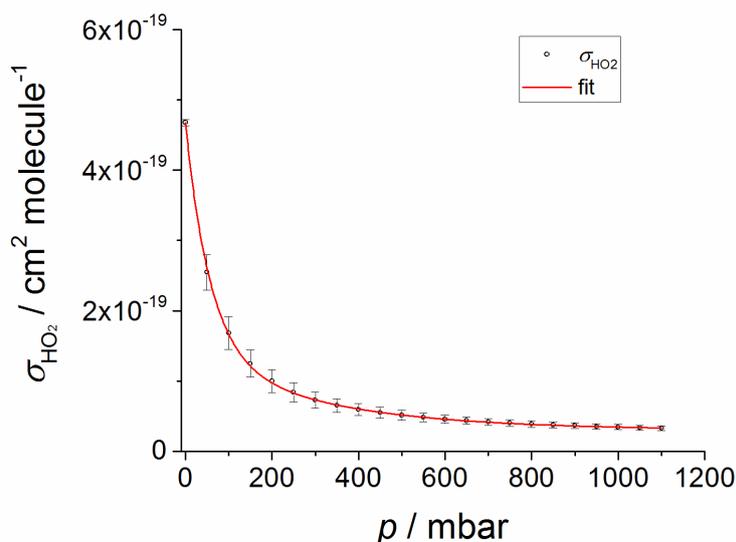
Figure 4: Absorption cross section of HO$_2$ at 1506.43 nm vs. pressure of air. The σ_{HO2} values (circles) were computed using the line strengths of the HO$_2$ transitions contributing to the absorption at 1506.43 nm (Thiebaud et al., 2007) and the pressure broadening coefficients assumed to be the same for all transitions and equal to the average of the values reported for the spectral region between 1499 and 1508 nm (0.115 cm^{-1} atm^{-1} = 1.14×10^{-4} cm^{-1} mbar^{-1}) (Ibrahim et al., 2007) as explained in the main text. The red line is a fit of Eq. (7) to the calculated values. The extracted values of the equation parameters are shown in Table S3 in the supplementary information.

3.3 Determination of σ_{HO_2} (1506.43 nm) using the kinetics of the HO₂ temporal decay

3.3.1 σ_{HO_2} (1506.43 nm) at 150 mbar

The kinetics of the temporal decay of HO₂ monitored by CRDS when the HIRAC lamps were extinguished, i.e. the HO₂

5 absorption coefficient at 1506.43 nm (α_{HO_2}) vs. time, has been used to determine σ_{HO_2} at 150 mbar. The absorption coefficient

α_{HO_2} (the product of the absorption cross section and the concentration) was computed using Eq. (9).

$$\alpha_{HO_2} = \frac{1}{c}\left(\frac{1}{\tau} - \frac{1}{\tau_0}\right), \tag{9}$$

10 where c is the velocity of light and τ and τ_0 are the ring-down times recorded with the lamps on and off, respectively.

The temporal decays of α_{HO_2} were analysed to extract σ_{HO_2} in a similar fashion to how the FAGE signal decays were analysed

to determine the FAGE calibration factor, C_{HO_2} (Eq. (4) in Section 2.3.2). Therefore, HO₂ decays were analysed using Eq. (10).

$$(\alpha_{HO_2})_t = \left(\left(\frac{1}{(\alpha_{HO_2})_0} + \frac{2 \cdot k_{self-r.}}{k_{loss} \cdot \sigma_{HO_2}}\right) \times \exp(k_{loss}t) - \left(\frac{2 \cdot k_{self-r.}}{k_{loss} \cdot \sigma_{HO_2}}\right)\right)^{-1}, \tag{10}$$

where k_{self-r} and k_{loss} have already been defined and $(\alpha_{HO_2})_t$ and $(\alpha_{HO_2})_0$ are the absorption coefficient at time t and $t = 0$ (the

15 time when the UV lamps were switched off). Eq. (10) was fitted to eight temporal traces (Fig. 5 shows an example) to obtain

an average $\sigma_{HO_2} = (1.02 \pm 0.18) \times 10^{-19}$ cm² molecule⁻¹ (see all the values in Table S4), where the error is a combination of

systematic and statistical uncertainties at the 1σ level. The obtained σ_{HO_2} is in good agreement with $\sigma_{HO_2} = (1.25 \pm 0.19) \times 10^{-19}$ cm² molecule⁻¹ generated by the analysis presented in Section 3.2, and $k_{loss} = (0.11 \pm 0.01)$ s⁻¹.
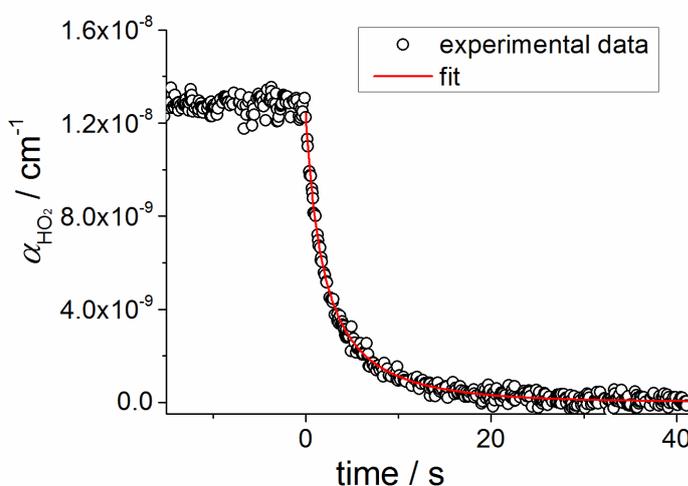
Figure 5: Second-order decay of the HO₂ absorption coefficient at 1506.43 nm obtained by CRDS. Experiments performed in
HIRAC at 295 K and 150 mbar mixture of N₂:O₂ = 4:1; [Cl₂]₀ ~ 1.5 × 10¹⁴ molecule cm⁻¹ and [CH₃OH]₀ ~ 1.0 × 10¹⁴ molecule
cm⁻³. At time zero the photolysis lamps were turned off. Fitting Eq. (10) to the data gave $\sigma_{HO_2} = (1.02 \pm 0.05) \times 10^{-19}$ cm²
molecule⁻¹ (statistical error at 1σ level).

3.3.2 σ_{HO2} (1506.43 nm) at 1000 mbar

The measured absorption coefficients $\alpha_{HO2, 1000\ mbar}$ were three times lower than $\alpha_{HO2, 150\ mbar}$ for the same HO$_2$ concentrations, hence the signal-to-noise ratio decreased with increasing pressure (see Figs. 5 and 6 as examples of α_{HO2} vs. time at the two pressures). Therefore, the statistical uncertainties in the kinetic analysis of the α_{HO2} temporal decays were relatively high at

5   1000 mbar, having values of ~ 14% in σ_{HO2} and ~ 22% in k_{loss} at 1σ level on average. By comparison, the precision of the kinetic method at 1σ level at 150 mbar was ~ 3% in $\sigma_{HO2, 150\ mbar}$ and ~ 6% in $k_{loss, 150\ mbar}$. In order to reduce the CRDS statistical uncertainties at 1000 mbar, the FAGE signal decays monitored at the same time with the α_{HO2} decays were used to determine σ_{HO2}(1000 mbar). In this approach the fluorescence signal decays were scaled to overlap α_{HO2} vs. time by multiplying the FAGE signal by $f = \frac{(\bar{\alpha}_{HO_2})_0}{(\bar{S}_{HO_2})_0}$, where $(\bar{\alpha}_{HO_2})_0$ and $(\bar{S}_{HO_2})_0$ are the mean absorption coefficient and the mean FAGE signal

10   before the UV lamps off are turned off. Equation 10, where $k_{self-r.}$ was fixed to 2.85×10^{-12} cm^{-3} molecule^{-1} s^{-1} (Atkinson et al., 2004), was fitted to the scaled signal decays (Fig. 6 shows an example) to obtain an average $\sigma_{HO2} = (3.87 \pm 0.74) \times 10^{-20}$ cm^2 molecule^{-1} (further details in supplementary information), where the error limits are overall errors quoted at 1σ level. The value broadly agrees with $\sigma_{HO2} = (3.44 \pm 0.37) \times 10^{-20}$ cm^2 molecule^{-1} computed by the model described in Section 3.2, which considered the contribution of the air-broadened HO$_2$ absorption lines (Thiebaud et al., 2007) to the overall cross section at

15   1506.43 nm.
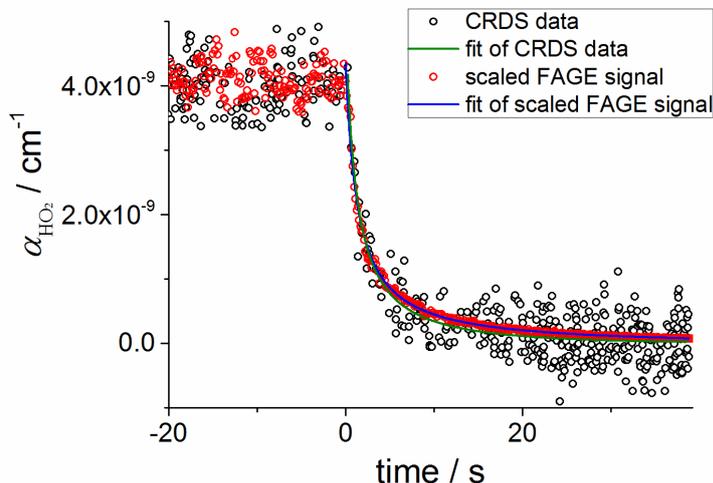
Figure 6: An example of a temporal decay of the HO$_2$ absorption coefficient at 1506.43 nm from CRDS data (black circles) along with the FAGE signal scaled to overlap the CRDS data (see text for details). The traces were recorded at 295 K and with

20   a 1000 mbar mixture of N$_2$:O$_2$ = 4:1; [Cl$_2$]$_0$ ~ 1.7×10^{14} molecule cm^{-3} and [CH$_3$OH]$_0$ ~ 2.0×10^{14} molecule cm^{-3}. The fit of Eq. (9) to the CRDS data (green line) gave $\sigma_{HO2} = (3.59 \pm 0.52) \times 10^{-20}$ cm^2 molecule^{-1} while the fit of Eq. (9) to the scaled FAGE data (blue line) resulted in $\sigma_{HO2} = (3.54 \pm 0.05) \times 10^{-20}$ cm^2 molecule^{-1}. The error limits are statistical errors at the 1σ level.

25   **3.4 Determination of the CRDS detection limits**

In order to quantify the sensitivity of the CRDS spectrometer the chamber was filled with synthetic air at 150 mbar and 1000 mbar, respectively and single ring-down events were continuously acquired at 1506.43 nm for 1.0 – 1.5 hour. As the CRDS noise increased slightly when the fans were turned on, separate measurements were performed where the fans were maintained

on and off, respectively. Fig. S4a in the supplementary information shows such separate measurements of the ring-down time at 1506.43 nm with the fans on and off, respectively as an example. The noise properties of the spectrometer can be characterized with an Allan deviation plot (Werle et al., 1993). The Allan variance, $\sigma_A^2(n)$, is the mean two-sample variance of pairs of adjacent points in a data series (absorption coefficients in our case), where each point is an average of n individual

5 measurements (ring-down events). The Allan deviation, $\sigma_A(n)$, is $(1/\sqrt{2})$ times the root-mean-square value of the difference between adjacent points. As such, the Allan deviation plot (Fig. 7 and Fig. S4b in the supplementary information) gives an estimate of the error, $\delta\alpha$, between successively measured absorption coefficients for a given averaging size n. At 1000 mbar, the optimum CRDS sensitivity is achieved by averaging ~ 600 ring-down events (requiring 60 s at an acquisition rate of 10 Hz), giving a minimum detectable absorption coefficient of $\delta\alpha_{min} = 2.6 \times 10^{-11}$ cm^{-1}. For n up to 3, the behaviour of $\sigma_A(n)$ is

10 that of white noise with a bandwidth-normalized value of 1.2×10^{-10} cm^{-1} Hz$^{-1/2}$. For n up to 100, the effect of excess noise is measurable but small, and for n larger than 100 the discrepancy becomes significant. At 150 mbar, the best sensitivity of $\delta\alpha_{min} = 1.5 \times 10^{-11}$ cm^{-1} is achieved after averaging ~ 250 events (25 s). The behaviour of $\sigma_A(n)$ is that of white noise for n up to 100, with a bandwidth-normalized value of 5.8×10^{-11} cm^{-1} Hz$^{-1/2}$.

For a signal-to-noise ratio (S/N) of 2, the limits of detection for HO$_2$, $LOD_{HO2} = (2\delta\alpha_{min})/\sigma_{HO2}$, where σ_{HO2} is the HO$_2$

15 cross section at 1506.43 nm the values shown in Table 1 were obtained.
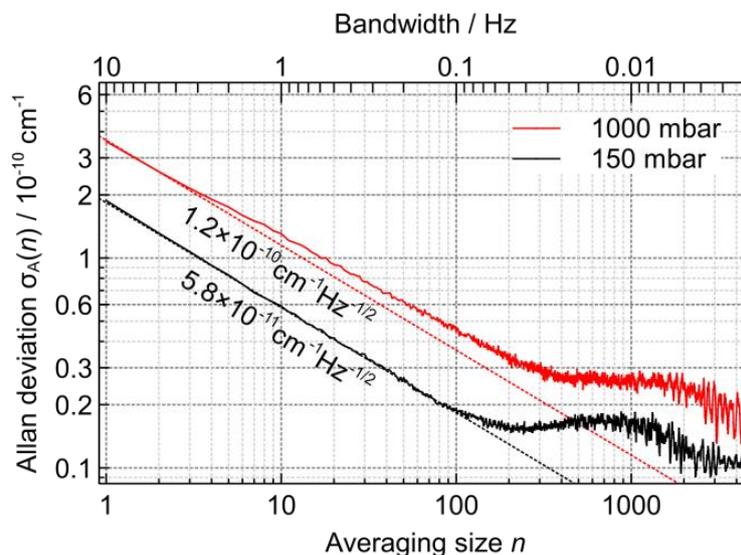
20 **Figure 7:** Allan deviation plot of the absorption coefficient at 1506.43 nm in the absence of HO$_2$ against the number of ring-down events averaged, n. For $S/N = 2$ the minimum detectable absorption coefficient for a single ring-down measurement is: 1.9×10^{-10} cm^{-1} at 150 mbar, which is reduced to 1.5×10^{-11} cm^{-1} after averaging 250 ring-down time constants, τ_0 (requiring 25 s at an acquisition rate of 10 Hz) and 3.6×10^{-10} cm^{-1} at 1000 mbar, which decreases to 2.7×10^{-11} cm^{-1} after $n = 600$ (requiring 60 s at an acquisition rate of 10 Hz).

25

Table 1. CRDS detection limits for HO$_2$ computed at 150 and 1000 mbar for single ring-down measurements (Δt = 0.1 s), the optimum averaging time, $\Delta t_{opt.}$, 25 s at 150 mbar and 60 s at 1000 mbar and two other averaging times: Δt = 3 s and Δt = 30 s.

p_{HIRAC} / mbar	$\sigma_{HO2} \times 10^{20}$ / cm^2 molecule^{-1}	$LOD_{HO2} \times 10^8$ / molecule cm^{-3}			
		Δt = 0.1 s	Δt = 3 s	Δt = 30 s	$\Delta t_{opt.}$
150	12.5 ± 1.9[a]	30.4	5.6	2.7	2.4
	10.2 ± 1.8[b]	37.3	6.8	3.3	2.9
1000	3.4 ± 0.4[a]	208	44.5	16.4	15.3
	3.9 ± 0.7[b]	185	39.4	14.6	13.3

[a] determined using the line strengths of the HO$_2$ transitions contributing to the absorption at 1506.43 nm (Thiebaud et al., 2007) and the pressure broadening coefficients (Ibrahim et al., 2007) (Section 3.2)

5 [b] determined using the kinetics of the HO$_2$ second-order decays (Section 3.3)

3.5 Intercomparison of CRDS and FAGE HO$_2$ measurements

3.5.1 150 mbar measurements

10 HO$_2$ was generated from photolysis of mixtures of Cl$_2$/CH$_3$OH/O$_2$ over a range of concentrations, ~ 6–750 × 10^8 molecule cm^{-3} at 150 mbar and ~ 4–100 × 10^9 molecule cm^{-3} at 1000 mbar. The comparison involved both periods with lamps on where [HO$_2$] was changing slowly and also where the lamps were turned off and the decay of HO$_2$ was followed. FAGE signals were converted into [HO$_2$] using the calibration constant determined in Sect. 2.3.2 using the kinetic decay of HO$_2$ ($C_{HO2,150\ mbar}$ = (2.6 ± 0.5) × 10^{-7} counts cm^3 molecule^{-1} s^{-1} mW^{-1}). CRDS absorptions were converted to concentrations based on either the cross-

15 section derived from the study of the recombination kinetics in section 3.3.1 ($\sigma_{HO2,\ 150\ mbar}$ = (1.02 ± 0.18) × 10^{-19} cm^2 molecule^{-1}), or the value of the cross-section determined by application of pressure broadening to the spectral lines reported by Thiebaud et al. (2007) (Sect. 3.2; $\sigma_{HO2,\ 150\ mbar}$ = (1.25 ± 0.19) × 10^{-19} cm^2 molecule^{-1}). Figure 8a shows an example of a typical temporal profile of absolute HO$_2$ concentrations recorded over ~ 15 minutes first with lamps on and then lamps switched off. The agreement between [HO$_2$] determined by the FAGE method and the CRDS method with the Thiebaud et al. based

20 cross-section is excellent (the difference is within 3%). Considering errors of approximately 20% in both the FAGE calibrations and absorption cross-section determined in the kinetic studies, then the FAGE determined HO$_2$ concentrations are also consistent with those from CRDS with our kinetically determined absorption cross-section. Figure 8b shows a correlation plot of the complete intercomparison dataset with the two different absorption cross-sections. The correlations are linear over the range of [HO$_2$], ~ 6–750 × 10^8 molecule cm^{-3}, (average gradient = 0.903 ± 0.002) with a very small negative intercept ((-1.0 ±

25 0.5) × 10^8 molecule cm^{-3}) which is insignificant compared to the typical HO$_2$ concentrations in this simulation chamber experiment.
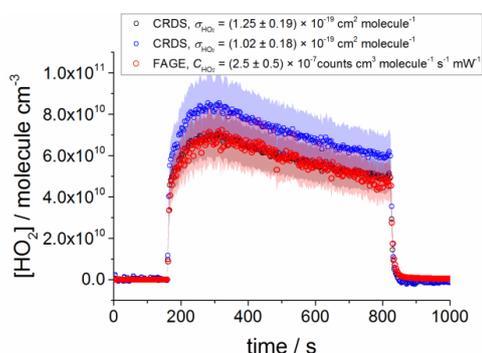
Figure 8a. Comparison HO₂ measurement at 150 mbar where the lamps were switched on at t = ~150 seconds for ~10 minutes. HO₂ measured by FAGE ($C_{150\ mbar} = 2.6 \times 10^{-7}$ counts cm³ molecule⁻¹ s⁻¹ mW⁻¹, red) is plotted with HO₂ measured by CRDS using $\sigma_{HO2} = 1.25 \times 10^{-19}$ cm² molecule⁻¹ obtained (Sect. 3.2) by application of pressure broadening to the spectral lines found by Thiebaud et al. (2017) (black), and $\sigma_{HO2} = 1.02 \times 10^{-19}$ cm² molecule⁻¹ determined using the kinetic decays of HO₂ in Sect. 3.3.1 (blue). Each datum point is an averaged value over 3 seconds. [CH₃OH] = 6.6×10^{13} molecule cm⁻³, [Cl₂] = 4.4×10^{13} molecule cm⁻³.
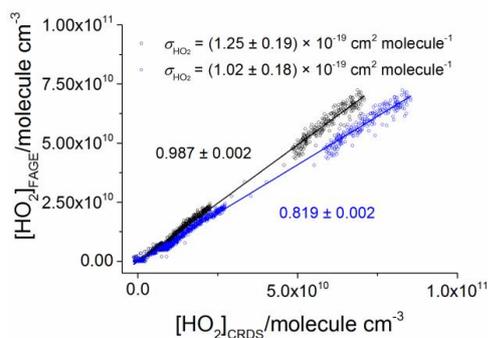
Figure 8b. Correlation plot at 150 mbar for data plotted in Fig. 8a. [HO₂]CRDS was calculated using $\sigma_{HO2} = 1.25 \times 10^{-19}$ cm² molecule⁻¹ determined in Sect. 3.2 (black) and $\sigma_{HO2} = 1.02 \times 10^{-19}$ cm² molecule⁻¹ determined in Sect. 3.3.1 (blue). Linear fits of the data generated gradients of 0.987 ± 0.002 and 0.819 ± 0.002 respectively. Both lines intercept the y axis at $(-1.0 \pm 0.5) \times 10^8$ molecule cm⁻³. [HO₂]FAGE was calculated using a sensitivity factor of 2.6×10^{-7} counts cm³ molecule⁻¹ s⁻¹ mW⁻¹ from the HO₂ decay as discussed in Sect. 2.3.2. Each datum point is an averaged value over 3 seconds.

3.5.2 1000 mbar measurements

Figures 9a and b show the equivalent comparisons for data recorded at 1000 mbar. Once again two values for the CRDS derived concentrations are given, firstly based on the pressure broadened cross-section of Thiebaud et al. (2007) ($\sigma_{HO2} = (3.44 \pm 0.37) \times 10^{-20}$ cm² molecule⁻¹) and secondly from the experimentally determined cross-sections using the HO₂ decay (section

5   3.3.2, $\sigma_{HO2} = (3.89 \pm 0.74) \times 10^{-20}$ cm² molecule⁻¹). The data are more scattered reflecting the lower sensitivity of the CRDS technique at 1000 mbar, but once again the HO₂ concentrations determined by the two techniques (with either cross-section) are consistent within the ~ 20% errors associated with the calibration of FAGE and the cross-section determinations (average gradient of the two correlation plots = 0.836 ± 0.004).
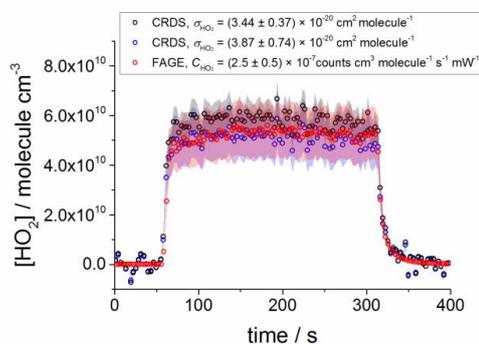
Figure 9a. Comparison measurement at 1000 mbar where the lamps were left on for ~ 4 minutes. HO_2 measured by FAGE using the calibration factor obtained as shown in Sect. 2.3.1: the average of the value determined by the H_2O photolysis and the value obtained using the HO_2 decays, $C_{1000\ mbar} = 2.5 \times 10^{-7}$ counts cm^3 molecule^{-1} s^{-1} mW^{-1}; red circles, is plotted with HO_2 measured by CRDS using $\sigma_{HO2} = 3.44 \times 10^{-19}$ cm^2 molecule^{-1} determined (Sect. 3.2) by application of pressure broadening to the spectral lines found by Thiebaud et al. (2017) (black circles), and $\sigma_{HO2} = 3.87 \times 10^{-20}$ cm^2 molecule^{-1} determined using the kinetic decays of HO_2 in Sect. 3.3.2 (blue circles). Each datum point is an averaged value over 3 seconds. $[CH_3OH] \sim 1.65 \times 10^{15}$ molecule cm^{-3}, and $[Cl_2] \sim 1.10 \times 10^{14}$ molecule cm^{-3}.
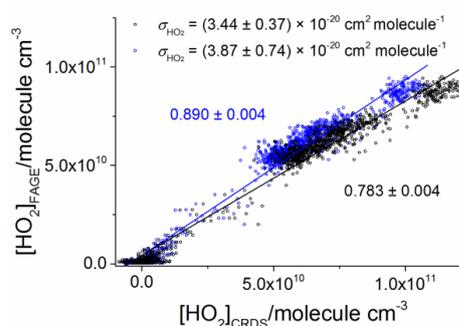
Figure 9b. Correlation plot at 1000 mbar for data in Fig. 9a. $[HO_2]_{CRDS}$ was calculated using $\sigma_{HO2} = 3.44 \times 10^{-20}$ cm^2 determined as shown in Sect. 3.2 (black) and $\sigma_{HO2} = 3.87 \times 10^{-20}$ cm^2 determined as shown in Sect. 3.3.2 (blue). Linear fits of the data generated gradients of 0.890 ± 0.004 and 0.783 ± 0.004 respectively, and an intercept of $(-4.3 \pm 0.3) \times 10^9$ and $(-1.0 \pm 0.5) \times 10^8$ molecule cm^{-3} respectively. $[HO_2]_{FAGE}$ was calculated using the sensitivity factor $\overline{C}_{1000\ mbar} = 2.5 \times 10^{-7}$ counts cm^3 molecule^{-1} s^{-1} mW^{-1}, which is the average of the value determined by the H_2O photolysis and the mean value determined using the HO_2 decays (Sect. 2.3.1). Each datum point is an averaged value over 3 seconds.

4 Discussion

The HO_2 near-IR absorption spectrum around 1506 nm recorded in this study using CRDS is in good agreement with previous work both in terms of the wavelength of the maximum absorption, and the cross-section at 150 mbar ($\sigma_{HO2,\ 150\ mbar}$), as

5   determined here by kinetics measurements. The $\sigma_{HO2,\ 150\ mbar}$ from the kinetics studies $(1.02 \pm 0.18) \times 10^{-19}$ cm^2 molecule^{-1} (Sect. 3.3.1) is within the error ranges of derived from two previous studies: (i) $\sigma_{HO2,\ 150\ mbar} = (1.25 \pm 0.19) \times 10^{-19}$ cm^2 molecule^{-1} computed using the 50 mbar He measurements of Thiebaud et al. (2007), where the line centres and strengths of the HO_2 transitions at ~ 1506.43 nm were extracted from the reported spectra and combined with the pressure broadening in air (Ibrahim et al., 2007) (Sect. 3.2) to give σ_{HO2} at 150 mbar, and (ii) $\sigma_{HO2,\ 150\ mbar} = (1.29 \pm 0.23) \times 10^{-19}$ cm^2 molecule^{-1} obtained

10   by extrapolating the cross-sections determined by Tang et al. (2010) in the range of 27–133 mbar. Significant pressure broadening is observed such that the lower cross-section at 1000 mbar, $\sigma_{HO2,\ 1000\ mbar}$, and hence reduced signal to noise, makes extraction of a precise σ_{HO2} using the CRDS data from the recombination kinetics difficult. However, a comparison of the temporal profiles of the HO_2 decays from CRDS and FAGE (e.g. Fig. 6) shows good agreement and the resulting absorption cross-section, an average from the analysis of 6 decays, $\sigma_{HO2} = (3.89 \pm 0.74) \times 10^{-20}$ cm^2 molecule^{-1}, is in good agreement with

15   the value of $\sigma_{HO2} = (3.44 \pm 0.37) \times 10^{-20}$ cm^2 molecule^{-1} obtained by application of pressure broadening to the data of Thiebaud et al. (2007).

       The good agreement (only ~ 10–15 % difference on average) between CRDS and FAGE for both the HO_2 concentrations with the lamps on and their temporal dependence when the lamps were switched off, as exemplified in Figs. 6, 8 and 9 (see also Figs. S7 and S8 in the supplementary information), provides validation between the absolute and direct

20   method of HO_2 detection via CRDS and the FAGE technique which is an indirect method requiring calibration. The CRDS method requires a known σ_{HO2} and this is non-trivial to obtain for a radical species, so there are systematic uncertainties of approximately 20% associated with CRDS measurements of HO_2. Whilst no significant concerns have been raised about either

the photolysis of water vapour at 185 nm in air as a method to generate HO_2 for calibration, or the indirect method of determining HO_2 by NO titration to OH (at least for the simple chemical environments described in this paper), this is the first direct, real time, quantitative intercomparison between CRDS and FAGE for HO_2 detection. The good agreement between the two techniques raises confidence for their application. Such a level of agreement provides evidence for there being no

5   undetected systematic errors in either technique. Note that this work also supports the method used to measure HO_2 via the CIMS technique as CIMS also relies on a similar methodology, namely titration with NO to convert HO_2 to OH (Edwards et al., 2003).

Table 2 compares the *LOD* of the CRDS system described here with the *LOD* values reported in previous studies using the first overtone of the O-H stretch in near IR to detect HO_2 through different techniques: CRDS (Thiebaud et al., 2007;Thiebaud

10   et al., 2008;Liu et al., 2008), noise-immune cavity-enhanced optical heterodyne molecular spectroscopy, NICE-OHMS (Bell et al., 2012) and wavelength modulation near IR spectroscopy, WM-NIR (Noell et al., 2010). The CRDS instrument used in this work allows for more sensitive measurements of HO_2 than in the above cited references. However, the instrument has insufficient sensitivity to detect ambient levels of HO_2, where typical maximum concentrations are very dependent upon NO_x and range from $(0.5 - 10) \times 10^8$ molecule cm^{-3} (Carslaw et al., 2001;Heard et al., 2004;Dusanter et al., 2009;Holland et al.,

15   2003) and ideally a detection limit $< 1 \times 10^7$ molecule cm^{-3} is required. However, the sensitivity (*LOD* for [HO_2] with 30 s averaging at 1000 mbar $\sim 1.5 \times 10^9$ molecule cm^{-3}) is more than adequate for chamber studies where in general [HO_2] $> 3 \times 10^{10}$ molecule cm^{-3} can be generated and 30 second averaging should provide good temporal resolution as experiments typically take between 10 and 120 minutes (Malkin et al., 2010;Winiberg et al., 2016). It is stressed however that the *LOD* quoted here is in the absence of water vapour. No change in the *LOD* at 150 mbar in the presence of typical ambient concentrations of

20   water (10^{17} molecule cm^{-3} orders of magnitude) is expected at 150 mbar as there is little overlap of the water absorption lines with the HO_2 absorption at 1506.43 nm at this pressure. However, in the presence of [H_2O] $\sim 10^{17}$ molecule cm^{-3} the CRDS sensitivity at 1000 mbar is expected to decrease markedly relative to the sensitivity in dry air found in this work due to the pressure broadening of the H_2O spectral lines resulting in a significant H_2O absorption at 1506.43 nm in the background of the HO_2 measurements.

25

30

35

40

Table 2. Comparison of the detection limits (LOD) for HO$_2$ obtained in this work with previously reported LOD (extrapolated to 30 s integration time, 0.033 Hz detection bandwidth) obtained by detecting HO$_2$ in near IR via the first vibrational overtone of the O-H stretch

LOD / molecule cm^{-3}	Wavelength / nm	Pressure / mbar	Bath gas	Technique	Reference
$8.0 \times 10^{8, a}$	1506.43	66.7	He	CRDS	Thiebaud et al., 2007
$5.8 \times 10^{8, b}$	1506.43	33.3	He	CRDS	Thiebaud et al., 2008
$\sim 1 \times 10^{11, c}$	1509.27 nm	40.0	N$_2$	CRDS	Liu et al., 2008
$\sim 8 \times 10^{9, d}$	1509.82 and 1509.76	53.3	Ar	NICE-OHMS	Bell et al., 2012
$\sim 1.8 \times 10^{10, e}$	1506.43	42.7 – 160.0	N$_2$/O$_2$/He	WM-NIR	Noell et al., 2010
$3.0 \times 10^{8, f}$	1506.43	150	air	CRDS	this work
$1.5 \times 10^{9, g}$	1506.43	1000	air	CRDS	this work

[a] Cavity ring-down spectroscopy (CRDS); Calculated for $\sigma_{HO2} = 2.7 \times 10^{-19}$ cm^2 molecule^{-1}; $\alpha_{min} = 1.2 \times 10^{-9}$ cm^{-1} Hz$^{-1/2}$

[b] Calculated for $\sigma_{HO2} = 3.4 \times 10^{-19}$ cm^2 molecule^{-1} and $\alpha_{min} = 1.1 \times 10^{-9}$ cm^{-1} Hz$^{-1/2}$

[c] LOD computed by using the noise level of the HO$_2$ spectrum baseline and corresponded to $\alpha_{min} \sim 3 \times 10^{-8}$ cm^{-1} for HO$_2$ generated in dielectric barrier discharge plasma; bandwidth unknown

[d] Noise-immune cavity-enhanced optical heterodyne molecular spectroscopy (NICE-OHMS); $\sigma_{HO2, 1509.82} = 9.7 \times 10^{-20}$ cm^2 molecule^{-1} and $\sigma_{HO2, 1509.76} = 1.3 \times 10^{-19}$ cm^2 molecule^{-1}; LOD calculated for a sensitivity of $\alpha_{HO2} = 5.7 \times 10^{-9}$ cm^{-1} Hz$^{-1/2}$

[e] Wavelength modulation near IR (WM-NIR) spectroscopy; LOD given as 1×10^{11} cm^{-3} Hz$^{-1/2}$; typical concentrations: $(3 – 15) \times 10^{16}$ molecule cm^{-3} He, $(5 – 20) \times 10^{17}$ molecule cm^{-3} O$_2$ and $(0-1) \times 10^{18}$ molecule cm^{-3} N$_2$

[f] Average of the two LOD shown in Table 1 (computed for $\sigma_{HO2} = 1.25 \times 10^{-19}$ cm^2 molecule^{-1} and $\sigma_{HO2} = 1.02 \times 10^{-19}$ cm^2 molecule^{-1}); $S/N = 2$

[g] Average of the two LOD shown in Table 1 (computed for $\sigma_{HO2} = 3.44 \times 10^{-20}$ cm^2 molecule^{-1} and $\sigma_{HO2} = 3.87 \times 10^{-20}$ cm^2 molecule^{-1}); $S/N = 2$

The CRDS sensitivity could be further optimised by setting up the CRDS along HIRAC to increase the cavity length to 2.0 m (from the present length of 1.4 m). Measurements of fast kinetic decays of HO$_2$ and averaging of ring-down events where HO$_2$ is in steady-state would benefit from an increase of the frequency of the ring-down events. No improvement of the sensitivity is expected by changing the wavelength of the measurements to another value in near IR as this work has been already performed at the wavelength of the most important HO$_2$ absorption feature (1506.43 nm) in the range of $\sim 1493 – 1514$ nm (vacuum wavelength corresponding to 6604–6696 cm^{-1}) where the first overtone of the O-H stretch has been observed (Thiebaud et al., 2007;DeSain et al., 2003). Even though the mid IR range provides stronger HO$_2$ absorption cross sections (Richard et al., 2012), the near IR region has been chosen for this study as it offers advantages such as improved performance of the detectors and optical components, which are also available at a lower cost.

In terms of practical operation, both the FAGE and CRDS methods require trained operatives and constant monitoring of conditions to ensure optimum performance; neither technique could be considered as a 'turn-key' process. The CRDS system does have a significant advantage in cost with the current apparatus being assembled for a cost of ~£ 9 k.

5 Conclusions

The Fluorescence Assay by Gas Expansion (FAGE) technique is the most commonly used method for the measurement of HO$_2$ in the atmosphere by conversion of HO$_2$ to OH by reaction with added NO followed by OH on-resonance LIF at 308 nm.

However, FAGE is not an absolute method and hence requires calibration. In this work an intercomparison is performed between the FAGE technique and the absolute Cavity Ring-Down Spectroscopy (CRDS) method within the Leeds HIRAC atmospheric simulation chamber. FAGE was conducted by sampling through a pinhole at ~ 0.2 m from the chamber wall (1.2 m internal diameter), while CRDS probed HO_2 over the entire width of the chamber, using the excitation of the first O-H

5   overtone at 1506.43 nm. The HO_2 radical was generated from photolysis of mixtures of $Cl_2/CH_3OH/O_2$ at room temperature and two total pressures (150 mbar and 1000 mbar of synthetic air) and was monitored simultaneously using the two techniques.

At 1000 mbar FAGE was calibrated using two different methods: the conventional calibration method consisting in the 185 nm photolysis of water vapour in synthetic air and the kinetic decay of the fluorescence signal method. The two methods were in agreement to within 8%; the average of the calibration factors obtained by the two methods was

10   $\overline{C}_{HO_2, 1000\ mbar}$=(2.5 ± 0.5) × 10^{-7} counts cm^3 molecule^{-1} s^{-1} mW^{-1}, which corresponds to a limit of detection (LOD) of 1.6 × 10^6 molecule cm^{-3} for a signal-to-noise (S/N) ratio of 2 and an averaging period of 30 s. At 150 mbar the kinetic method was used for FAGE calibration, which yielded C_{HO_2} = (2.6 ± 0.5) × 10^{-7} counts cm^3 molecule^{-1} s^{-1} mW^{-1} and, hence a LOD similar to that obtained at 1000 mbar. The HO_2 absorption cross section at 1506.43 nm, σ_{HO_2}, at 150 and 1000 mbar was determined using two independent methods: from the 50 mbar He measurements of Thiebaud et al. (2007), where the line centres and

15   strengths of the HO_2 transitions at ~ 1506.43 nm were extracted from the reported spectra and combined with the pressure broadening in air (Ibrahim et al., 2007), and from the kinetics of the second-order HO_2 decays. At each operating pressure the values of σ_{HO_2} obtained by the two methods agree with each other (within ~12% agreement at 1000 mbar and within ~20% agreement at 150 mbar). For a time resolution of 30 s the computed CRDS sensitivity using the Allan deviation plots and the average σ_{HO_2} at each pressure are: 3.0 × 10^8 at 150 mbar and 1.5 × 10^9 molecule cm^{-3} at 1000 mbar.

20   The comparison was performed for both periods where [HO_2] was decreasing slowly for 5–10 min and periods where the lamps were shortly turned on and then off to generate a series of HO_2 decays to encompass a wide range of [HO_2]: ~ 6–750 × 10^8 molecule cm^{-3} at 150 mbar and ~ 4–100 × 10^9 molecule cm^{-3} at 1000 mbar. The correlation plots at both pressures show a good agreement between [HO_2] measured using the indirect FAGE method and the direct CRDS method: a gradient of 0.987 ± 0.002 when σ_{HO_2} determined by application of pressure broadening to the reported spectral lines (Thiebaud et al., 2007) was

25   used at 150 mbar and average gradients (of the results obtained using the two σ_{HO_2} values at each pressure) of 0.903 ± 0.002 at 150 mbar and of 0.836 ± 0.004 at 1000 mbar. This intercomparison study provides a validation for the FAGE method and supports the use of the method employing CIMS for HO_2 measurements, which also relies on the conversion of HO_2 to OH by titration with NO (Edwards et al., 2003).

30   **References**

Atkinson, R., Baulch, D. L., Cox, R. A., Crowley, J. N., Hampson, R. F., Hynes, R. G., Jenkin, M. E., Rossi, M. J., and Troe, J.: Evaluated kinetic and photochemical data for atmospheric chemistry: Volume I - gas phase reactions of O_x, HO_x, NO_x and SO_x species, Atmos. Chem. Phys., 4, 1461-1738, 10.5194/acp-4-1461-2004, 2004.
Bell, C. L., van Helden, J. P. H., Blaikie, T. P. J., Hancock, G., van Leeuwen, N. J., Peverall, R., and Ritchie, G. A. D.: Noise-Immune
35   Cavity-Enhanced Optical Heterodyne Detection of HO_2 in the Near-Infrared Range, J. Phys. Chem. A, 116, 5090-5099, 10.1021/jp301038r, 2012.
Blin-Simiand, N., Pasquiers, S., and Magne, L.: Removal of formaldehyde by a pulsed dielectric barrier discharge in dry air in the 20 degrees C to 300 degrees C temperature range, J. Phys. D Appl. Phys, 49, 10.1088/0022-3727/49/19/195202, 2016.
Blocquet, M., Schoemaecker, C., Amedro, D., Herbinet, O., Battin-Leclerc, F., and Fittschen, C.: Quantification of OH and HO_2 radicals
40   during the low-temperature oxidation of hydrocarbons by Fluorescence Assay by Gas Expansion technique, P. Natl. Acad. Sci. USA, 110, 20014-20017, 10.1073/pnas.1314968110, 2013.
Bloss, W. J., Lee, J. D., Johnson, G. P., Sommariva, R., Heard, D. E., Saiz-Lopez, A., Plane, J. M. C., McFiggans, G., Coe, H., Flynn, M., Williams, P., Rickard, A. R., and Fleming, Z. L.: Impact of halogen monoxide chemistry upon boundary layer OH and HO_2 concentrations at a coastal site, Geophys. Res. Lett., 32, 10.1029/2004gl022084, 2005.
45   Brown, S. S.: Absorption spectroscopy in high-finesse cavities for atmospheric studies, Chem. Rev., 103, 5219-5238, 10.1021/cr020645c, 2003.
Brumfield, B., Sun, W. T., Ju, Y. G., and Wysocki, G.: Direct In Situ Quantification of HO_2 from a Flow Reactor, J. Phys. Chem. Lett., 4, 872-876, 10.1021/jz400143c, 2013.

Cantrell, C. A., and Stedman, D. H.: A possible technique for the measurement of atmospheric peroxy-radicals, Geophys. Res. Lett., 9, 846-849, 10.1029/GL009i008p00846, 1982.

Cantrell, C. A., Stedman, D. H., and Wendel, G. J.: Measurement of atmospheric peroxy-radicals by chemical amplification, Anal. Chem., 56, 1496-1502, 10.1021/ac00272a065, 1984.

5   Carslaw, N., Creasey, D. J., Harrison, D., Heard, D. E., Hunter, M. C., Jacobs, P. J., Jenkin, M. E., Lee, J. D., Lewis, A. C., Pilling, M. J., Saunders, S. M., and Seakins, P. W.: OH and HO_2 radical chemistry in a forested region of north-western Greece, Atmos. Environ., 35, 4725-4737, 2001.

Chen, D. X., Huey, L. G., Tanner, D. J., Li, J. F., Ng, N. L., and Wang, Y. H.: Derivation of Hydroperoxyl Radical Levels at an Urban Site via Measurement of Pernitric Acid by Iodide Chemical Ionization Mass Spectrometry, Environ. Sci. Technol., 51, 3355-3363, 10   10.1021/acs.est.6b05169, 2017.

Chen, Y., Yang, C., Zhao, W., Fang, B., Xu, X., Gai, Y., Lin, X., Chen, W., and Zhang, W.: Ultra-sensitive measurement of peroxy radicals by chemical amplification broadband cavity-enhanced spectroscopy, Analyst, 141, 5870-5878, 10.1039/c6an01038e, 2016.

Christensen, L. E., Okumura, M., Sander, S. P., Friedl, R. R., Miller, C. E., and Sloan, J. J.: Measurements of the rate constant of HO_2+NO_2 = HO_2NO_2 using near-infrared wavelength-modulation spectroscopy and UV-visible absorption spectroscopy, J. Phys. Chem. A, 108, 80-15   91, 10.1021/jp035905o, 2004.

DeSain, J. D., Ho, A. D., and Taatjes, C. A.: High-resolution diode laser absorption spectroscopy of the O-H stretch overtone band (2,0,0)<-(0,0,0) of the HO2 radical, J. Mol. Spectrosc., 219, 163-169, 10.1016/s0022-2852(03)00022-5, 2003.

Djehiche, M., Tomas, A., Fittschen, C., and Coddeville, P.: First Cavity Ring-Down Spectroscopy HO_2 Measurements in a Large Photoreactor, Z. Phys. Chem., 225, 983-992, 10.1524/zpch.2011.0143, 2011.

20   Djehiche, M., Tan, N. L. L., Jain, C. D., Dayma, G., Dagaut, P., Chauveau, C., Pillier, L., and Tomas, A.: Quantitative Measurements of HO_2 and Other Products of n-Butane Oxidation (H_2O_2, H_2O, CH_2O, and C_2H_4) at Elevated Temperatures by Direct Coupling of a Jet-Stirred Reactor with Sampling Nozzle and Cavity Ring-Down Spectroscopy (cw-CRDS), J. Am. Chem. Soc., 136, 16689-16694, 10.1021/ja510719k, 2014.

Dusanter, S., Vimal, D., Stevens, P. S., Volkamer, R., and Molina, L. T.: Measurements of OH and HO_2 concentrations during the MCMA-25   2006 field campaign - Part 1: Deployment of the Indiana University laser-induced fluorescence instrument, Atmos. Chem. Phys., 9, 1665-1685, 2009.

Edwards, G. D., Cantrell, C. A., Stephens, S., Hill, B., Goyea, O., Shetter, R. E., Mauldin, R. L., Kosciuch, E., Tanner, D. J., and Eisele, F. L.: Chemical ionization mass spectrometer instrument for the measurement of tropospheric HO_2 and RO_2, Anal. Chem., 75, 5317-5327, 10.1021/ac034402b, 2003.

30   Fittschen, C.: personal communication, 2017.

Fuch
s, H., Holland, F., and Hofzumahaus, A.: Measurement of tropospheric RO_2 and HO_2 radicals by a laser-induced fluorescence instrument, Rev. Sci. Instrum., 79, 10.1063/1.2968712, 2008.

Fuchs, H., Brauers, T., Haeseler, R., Holland, F., Mihelcic, D., Muesgen, P., Rohrer, F., Wegener, R., and Hofzumahaus, A.: Intercomparison 35   of peroxy radical measurements obtained at atmospheric conditions by laser-induced fluorescence and electron spin resonance spectroscopy, Atmos. Meas. Tech., 2, 55-64, 2009.

Fuchs, H., Brauers, T., Dorn, H. P., Harder, H., Haseler, R., Hofzumahaus, A., Holland, F., Kanaya, Y., Kajii, Y., Kubistin, D., Lou, S., Martinez, M., Miyamoto, K., Nishida, S., Rudolf, M., Schlosser, E., Wahner, A., Yoshino, A., and Schurath, U.: Technical Note: Formal blind intercomparison of HO_2 measurements in the atmosphere simulation chamber SAPHIR during the HOxComp campaign, Atmos. Chem. 40   Phys., 10, 12233-12250, 10.5194/acp-10-12233-2010, 2010.

Fuchs, H., Bohn, B., Hofzumahaus, A., Holland, F., Lu, K. D., Nehr, S., Rohrer, F., and Wahner, A.: Detection of HO_2 by laser-induced fluorescence: calibration and interferences from RO_2 radicals, Atmos. Meas. Tech., 4, 1209-1225, 10.5194/amt-4-1209-2011, 2011.

Gianella, M., Reuter, S., Aguila, A. L., Ritchie, G. A. D., and van Helden, J. P. H.: Detection of HO_2 in an atmospheric pressure plasma jet using optical feedback cavity-enhanced absorption spectroscopy, New J. Phys., 18, 10.1088/1367-2630/18/11/113027, 2016.

45   Glowacki, D. R., Goddard, A., Hemavibool, K., Malkin, T. L., Commane, R., Anderson, F., Bloss, W. J., Heard, D. E., Ingham, T., Pilling, M. J., and Seakins, P. W.: Design of and initial results from a Highly Instrumented Reactor for Atmospheric Chemistry (HIRAC), Atmos. Chem. Phys., 7, 5371-5390, 2007.

Green, T. J., Reeves, C. E., Fleming, Z. L., Brough, N., Rickard, A. R., Bandy, B. J., Monks, P. S., and Penkett, S. A.: An improved dual channel PERCA instrument for atmospheric measurements of peroxy radicals, J. Environ. Monitor., 8, 530-536, 10.1039/b514630e, 2006.

50   Hanke, M., Uecker, J., Reiner, T., and Arnold, F.: Atmospheric peroxy radicals: ROXMAS, a new mass-spectrometric methodology for speciated measurements of HO_2 and ΣRO_2 and first results, Int. J. Mass Spectrom., 213, 91-99, 10.1016/s1387-3806(01)00548-6, 2002.

Hard, T. M., Chan, C. Y., Mehrabzadeh, A. A., and Obrien, R. J.: Diurnal HO_2 Cycles at Clean-air and Urban Sites in the Troposphere, J. Geophys. Res-Atmos., 97, 9785-9794, 1992.

Heard, D. E., and Pilling, M. J.: Measurement of OH and HO_2 in the troposphere, Chem. Rev., 103, 5163-5198, 10.1021/cr020522s, 2003.

55   Heard, D. E., Carpenter, L. J., Creasey, D. J., Hopkins, J. R., Lee, J. D., Lewis, A. C., Pilling, M. J., Seakins, P. W., Carslaw, N., and Emmerson, K. M.: High levels of the hydroxyl radical in the winter urban troposphere, Geophys. Res. Lett., 31, L18112, 2004.

Holland, F., Hofzumahaus, A., Schafer, R., Kraus, A., and Patz, H. W.: Measurements of OH and HO_2 radical concentrations and photolysis frequencies during BERLIOZ, J. Geophys. Res-Atmos., 108, 10.1029/2001jd001393, 2003.

Ibrahim, N., Thiebaud, J., Orphal, J., and Fittschen, C.: Air-broadening coefficients of the HO_2 radical in the $2\nu_1$ band measured using cw-60   CRDS, J. Mol. Spectrosc., 242, 64-69, 10.1016/j.jms.2007.02.007, 2007.

Kircher, C. C., and Sander, S. P.: Kinetics and mechanism of HO_2 and DO_2 disproportionations, J. Phys. Chem-US, 88, 2082-2091, 10.1021/j150654a029, 1984.

Kurimoto, N., Brumfield, B., Yang, X. L., Wada, T., Dievart, P., Wysocki, G., and Ju, Y. G.: Quantitative measurements of HO_2/H_2O_2 and intermediate species in low and intermediate temperature oxidation of dimethyl ether, P. Combust. Inst., 35, 457-464, 65   10.1016/j.proci.2014.05.120, 2015.

Levy, H.: Normal Atmosphere - Large Radical and Formaldehyde Concentrations Predicted, Science, 173, 141-&, 10.1126/science.173.3992.141, 1971.

Liu, Z. W., Xu, Y., Yang, X. F., Zhu, A. M., Zhao, G. L., and Wang, W. G.: Determination of the HO_2 radical in dielectric barrier discharge plasmas using near-infrared cavity ring-down spectroscopy, J. Phys. D. Appl. Phys, 41, 10.1088/0022-3727/41/4/045203, 2008.

70   Lu, K. D., Rohrer, F., Holland, F., Fuchs, H., Bohn, B., Brauers, T., Chang, C. C., Haseler, R., Hu, M., Kita, K., Kondo, Y., Li, X., Lou, S. R., Nehr, S., Shao, M., Zeng, L. M., Wahner, A., Zhang, Y. H., and Hofzumahaus, A.: Observation and modelling of OH and HO_2

concentrations in the Pearl River Delta 2006: a missing OH source in a VOC rich atmosphere, Atmos. Chem. Phys., 12, 1541-1569, 10.5194/acp-12-1541-2012, 2012.

Malkin, T. L., Goddard, A., Heard, D. E., and Seakins, P. W.: Measurements of OH and HO_2 yields from the gas phase ozonolysis of isoprene, Atmos. Chem. Phys., 10, 1441-1459, 2010.

5 Mihelcic, D., Ehhalt, D. H., Klomfass, J., Kulessa, G. F., Schmidt, U., and Trainer, M.: Measurements of free-radicals in atmosphere by matrix-isolation and electron-paramagnetic resonance, Ber. Bunsen-Ges. Phys. Chem. Chem. Phys., 82, 16-19, 1978.

Miyazaki, K., Parker, A. E., Fittschen, C., Monks, P. S., and Kajii, Y.: A new technique for the selective measurement of atmospheric peroxy radical concentrations of HO_2 and RO_2 using a denuding method, Atmos. Meas. Tech., 3, 1547-1554, 10.5194/amt-3-1547-2010, 2010.

Morajkar, P., Schoemaecker, C., Okumura, M., and Fittschen, C.: Direct Measurement of the Equilibrium Constants of the Reaction of
10 Formaldehyde and Acetaldehyde with HO_2 Radicals, Int. J. Chem. Kinet., 46, 245-259, 10.1002/kin.20817, 2014.

Noell, A. C., Alconcel, L. S., Robichaud, D. J., Okumura, M., and Sander, S. P.: Near-Infrared Kinetic Spectroscopy of the HO_2 and $C_2H_5O_2$ Self-Reactions and Cross Reactions, J. Phys. Chem. A, 114, 6983-6995, 10.1021/jp912129j, 2010.

O'Keefe, A., and Deacon, D. A. G.: Cavity Ring-Down Optical Spectrometer for Absorption-measurements Using Pulsed Laser Sources, Rev. Sci. Instrum., 59, 2544-2551, 1988.

15 Onel, L., Brennan, A., Seakins, P. W., Whalley, L., and Heard, D. E.: A new method for atmospheric detection of the CH_3O_2 radical, Atmos. Meas. Tech. Discuss., doi:10.5194/amt-2017-5122, 2017.

Parker, A. E., Jain, C., Schoemaecker, C., Szriftgiser, P., Votava, O., and Fittschen, C.: Simultaneous, time-resolved measurements of OH and HO_2 radicals by coupling of high repetition rate LIF and cw-CRDS techniques to a laser photolysis reactor and its application to the photolysis of H_2O_2, Appl. Phys. B-Lasers O., 103, 725-733, 10.1007/s00340-010-4225-1, 2011.

20 Ren, X. R., Edwards, G. D., Cantrell, C. A., Lesher, R. L., Metcalf, A. R., Shirley, T., and Brune, W. H.: Intercomparison of peroxy radical measurements at a rural site using laser-induced fluorescence and Peroxy Radical Chemical Ionization Mass Spectrometer (PerCIMS) techniques, J. Geophys. Res-Atmos., 108, 10.1029/2003jd003644, 2003.

Richard, C., Gordon, I. E., Rothman, L. S., Abel, M., Frommhold, L., Gustafsson, M., Hartmann, J. M., Hermans, C., Lafferty, W. J., Orton, G. S., Smith, K. M., and Tran, H.: New section of the HITRAN database: Collision-induced absorption (CIA), J. Quant. Spectrosc. Ra., 113,
25 1276-1285, 10.1016/j.jqsrt.2011.11.004, 2012.

Sanchez, J., Tanner, D. J., Chen, D. X., Huey, L. G., and Ng, N. L.: A new technique for the direct detection of HO_2 radicals using bromide chemical ionization mass spectrometry (Br-CIMS): initial characterization, Atmos. Meas. Tech., 9, 3851-3861, 10.5194/amt-9-3851-2016, 2016.

Schocker, A., Uetake, M., Kanno, N., Koshi, M., and Tonokura, K.: Kinetics and rate constants of the reaction $CH_2OH+O_2 \rightarrow CH_2O+HO_2$
30 in the temperature range of 236-600 K, J. Phys. Chem. A, 111, 6622-6627, 10.1021/jp0682513, 2007.

Stone, D., Whalley, L. K., and Heard, D. E.: Tropospheric OH and HO_2 radicals: field measurements and model comparisons, Chem. Soc. Rev., 41, 6348-6404, 10.1039/c2cs35140d, 2012.

Taatjes, C. A., and Oh, D. B.: Time-resolved wavelength modulation spectroscopy measurements of HO_2 kinetics, Appl. Optics, 36, 5817-5821, 10.1364/ao.36.005817, 1997.

35 Tang, Y. X., Tyndall, G. S., and Orlando, J. J.: Spectroscopic and Kinetic Properties of HO_2 Radicals and the Enhancement of the HO_2 Self Reaction by CH_3OH and H_2O, J. Phys. Chem. A, 114, 369-378, 10.1021/jp905279b, 2010.

Thiebaud, J., and Fittschen, C.: Near infrared cw-CRDS coupled to laser photolysis: Spectroscopy and kinetics of the HO_2 radical, Appl. Phys. B-Lasers O., 85, 383-389, 10.1007/s00340-006-2304-0, 2006.

Thiebaud, J., Crunaire, S., and Fittschen, C.: Measurements of line strengths in the 2 v_1 band of the HO_2 radical using laser
40 photolysis/continuous wave cavity ring-down spectroscopy (cw-CRDS), J. Phys. Chem. A, 111, 6959-6966, 10.1021/jp0703307, 2007.

Thiebaud, J., Parker, A., Fittschen, C., Vincent, G., Zahraa, O., and Marquaire, P. M.: Detection of HO_2 radicals in the photocatalytic oxidation of methyl ethyl ketone, J. Phys. Chem. C, 112, 2239-2243, 10.1021/jp711388k, 2008.

Werle, P., Mucke, R., and Slemr, F.: The limits of signal averaging in atmospheric trace-gas monitoring by Tunable Diode-Laser Absorption Spectroscopy (TDLAS), Appl. Phys. B-Photo., 57, 131-139, 10.1007/bf00425997, 1993.

45 Whalley, L. K., Blitz, M. A., Desservettaz, M., Seakins, P. W., and Heard, D. E.: Reporting the sensitivity of laser-induced fluorescence instruments used for HO_2 detection to an interference from RO_2 radicals and introducing a novel approach that enables HO_2 and certain RO_2 types to be selectively measured, Atmos. Meas. Tech., 6, 3425-3440, 10.5194/amt-6-3425-2013, 2013.

Wheeler, M. D., Newman, S. M., Orr-Ewing, A. J., and Ashfold, M. N. R.: Cavity ring-down spectroscopy, J. Chem. Soc. Faraday T., 94, 337-351, 1998.

50 Winiberg, F. A. F., Smith, S. C., Bejan, I., Brumby, C. A., Ingham, T., Malkin, T. L., Orr, S. C., Heard, D. E., and Seakins, P. W.: Pressure-dependent calibration of the OH and HO_2 channels of a FAGE HO_x instrument using the Highly Instrumented Reactor for Atmospheric Chemistry (HIRAC), Atmos. Meas. Tech., 8, 523-540, 10.5194/amt-8-523-2015, 2015.

Winiberg, F. A. F., Dillon, T. J., Orr, S. C., Gross, C. B. M., Bejan, I., Brumby, C. A., Evans, M. J., Smith, S. C., Heard, D. E., and Seakins, P. W.: Direct measurements of OH and other product yields from the $HO_2 + CH_3C(O)O_2$ reaction, Atmos. Chem. Phys., 16, 4023-4042, 2016.

55 Yamada, C., Endo, Y., and Hirota, E.: Difference frequency laser spectroscopy of the v_1 band of the HO_2 radical, J. Chem. Phys., 78, 4379-4384, 10.1063/1.445321, 1983.

Zador, J., Taatjes, C. A., and Fernandes, R. X.: Kinetics of elementary reactions in low-temperature autoignition chemistry, Prog. Energ. Combust., 37, 371-421, 10.1016/j.pecs.2010.06.006, 2011.

Zahniser, M. S., and Stanton, A. C.: A measurement of the vibrational band strength for the v_3 band of the HO_2 radical, J. Chem. Phys., 80,
60 4951-4960, 10.1063/1.446517, 1984.